High-Performance Multi-Resonance Thermally Activated Delayed Fluorescence Emitters for Narrowband Organic Light-Emitting Diodes

He Jiang[1,2], Jibiao Jin[1,2], Wai-Yeung Wong[1,2]**

[1] Department of Applied Biology and Chemical Technology and Research Institute for Smart Energy, The Hong Kong Polytechnic University, Hung Hom, Hong Kong, P. R. China.
E-mail: jibiao.jin@polyu.edu.hk; wai-yeung.wong@polyu.edu. hk
[2] The Hong Kong Polytechnic University Shenzhen Research Institute, Shenzhen 518057, P. R. China

Keywords: thermally activated delayed fluorescence, multi-resonance, organic light-emitting diodes, reverse intersystem crossing rate, narrowband emission

Multi-resonance thermally activated delayed fluorescence (MR-TADF) emitters have drawn considerable attention because of their remarkable optoelectronic properties of high emission efficiency and narrow emission profile, and represent an active subject of cutting-edge research in the organic electroluminescence (EL). However, the slow reverse intersystem crossing (RISC) rate of MR-TADF emitter caused by the large energy gap (ΔE_{ST}) and small spin-orbit coupling (SOC) matrix elements between the singlet and triplet excited states limits their further development in organic EL device. Currently, innovative molecular design strategies have been developed including the heavy atom integration, π-extended MR framework and metal perturbation and so on to improve the RISC process of MR-TADF emitters for high-performance EL devices. Here, we present an overview on the recent progress of MR-TADF emitters with fast RISC rate ($> 10^{-5}$ s^{-1}), with particular attention to the molecular design, optoelectronic properties and device performance of organic light-emitting diodes (OLEDs), which intends to systematize our knowledge in this subject for the thriving development of highly efficient MR-TADF emitters. Finally, the challenges and future prospects of MR-TADF materials are discussed comprehensively.

1. Introduction

The development of the flexible organic light-emitting diodes (OLEDs) has flourished for decades since the pioneering work reported by Tang and Vanslyke in 1980s, due to the tremendous potential of OLEDs in the fields of flat-panel display and solid-light lighting.[1-5] To

promote the performance of the OLEDs, extensive efforts have been made in the development of high-performance organic emitters, which should possess high exciton utilization for high device efficiency and narrow emission profile for high emission color purity.[6-10] According to the spin statics under the electrical excitation, singlet (S_1) and triplet (T_1) excitons are generated in a ratio of 1:3.[11-13] Therefore, the way to utilize the inevitably formed nonemissive T_1 excitons becomes a hot research topic in the electroluminescence (EL) materials. By using the noble-metal atoms such as iridium (Ir) or platinum (Pt) to significantly enhance the spin-orbital coupling (SOC), both S_1 and T_1 excitons can be harvested efficiently for phosphorescence, realizing 100% internal quantum efficiency in theory.[14-16] However, these phosphors generally contain rare noble metal with high cost and this would become a challenge when OLED goes into mass production. Since the thermally activated delayed fluorescence (TADF) emitter based OLED was first reported in 2009,[17] TADF molecules have been extensively studied as one of the most promising emitters in EL devices.[18-20]

TADF emitters can harvest both S_1 and T_1 excitons via efficient reverse intersystem crossing (RISC) process by virtue of a small singlet-triplet energy gap (ΔE_{ST}).[21-23] A common strategy to obtain a small ΔE_{ST} is by integrating donor (D) and acceptor (A) groups into one molecule in a twisted molecular configuration for the well-separated highest occupied molecular orbital (HOMO) and lowest unoccupied molecular orbital (LUMO) (**Figure 1a**).[24-26] However, such a structure usually exhibits strong intramolecular charge transfer (ICT) and inevitably results in a large structural displacement between the ground state (S_0) and S_1, giving rise to a large Stokes shift and a broad emission profile, whose full width at half maximum (FWHM) typically exceeds 70 nm, degrading the emission color purity.[25, 27-30] Thus, developing a new type of materials with narrowband emission is quite vital to break through the intrinsic limitation of traditional TADF molecules.

Recently, Hatakeyama et al. proposed an innovate molecular design by constructing heteroatom embedded polycyclic aromatic hydrocarbons (PAHs) (**Figure 1b**), and such formed rigid molecular framework would induce a narrow emission owing to the suppression of vibronic coupling between S_0 and S_1 as well as the structural relaxation of S_1 (**Figure 1c**).[31-34] In this molecular design, the electron-donating atoms are introduced at the ortho positions of the electron-withdrawing atom in a fused polycyclic aromatic skeleton, inducing alternative distributions of the HOMO and LUMO wave functions in the aromatic framework because of the opposite resonance effect of the electrophilic atom and electron-donating atoms, making the resultant molecules to possess a moderate ΔE_{ST} and large emission oscillator strength for highly efficient TADF properties.[35-39] The newly designed molecules are known as multi-resonance

TADF (MR-TADF) emitters, which showed sharp emission profile with full width at half-maximum (FWHM) as narrow as 30 nm and excellent device performance with external quantum efficiencies (EQEs) beyond 30%.[37, 40, 41] However, MR-TADF molecules usually exhibit small RISC rate constant (< 10^5 s^{-1}) owing to the large ΔE_{ST} (≈ 0.2 eV) and small SOC matrix elements (< 0.1 cm^{-1}) between S_1 and T_1, leading to a large efficiency roll-off of the EL device.[42-47] In order to overcome this major challenge and motivate the flourishing development of MR-TADF materials, several kinds of molecular design strategies, such as the incorporation of heavy atom[48-51], metal perturbation[52] and π-extension of MR skeleton[32, 53-55] and so on, have been proposed (**Figure 1c**).

In this review, we systematically summarize the recent progress of MR-TADF materials with fast RISC rate constant (>10^5 s^{-1}) from the perspective of molecular design, optoelectronic properties and device performance of OLEDs. Furthermore, we provide our conclusions and future prospects on the remaining challenges in this research area to well promote the rapid development of high-performance OLEDs. A primary goal of this review is to summarize our knowledge in this area, extracting fundamental design principles of MR-TADF molecules with fast RISC rate, thus for the further understanding on the structure-performance relationship between the molecular structures of MR-TADF emitters and their OLED performances.

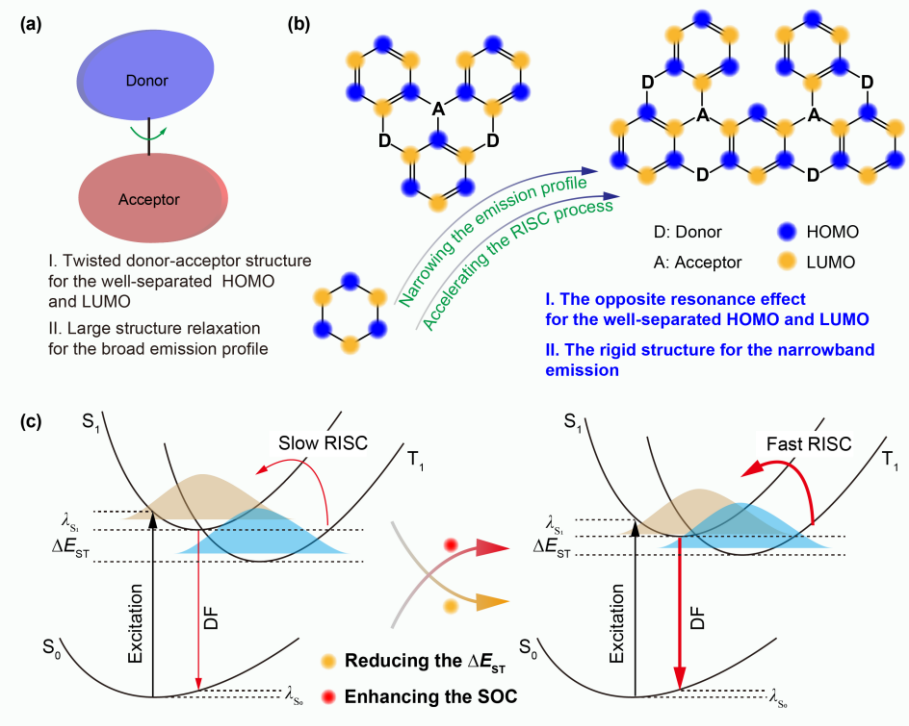

Figure 1. The molecular design strategies of (a) D-A type and (b) MR TADF molecules. (c) Schematic strategy to accelerate the RISC process of MR-TADF molecules by reducing the ΔE_{ST} and enhancing the SOC matrix elements.

2. The strategies for accelerating the RISC process

For the EL process of MR-TADF emitters, singlet and triplet excitons are firstly generated in a ratio of 1:3 according to the spin statistics.[56-58] Then, a part of singlet excitons can be converted to photons by radiative decay for prompt fluorescence (PF), another part of singlet excitons undergo nonradiative decay or transfer into triplet state through the intersystem crossing (ISC) process.[59, 60] Meanwhile, the triplet excitons can up-convert to the emissive singlet state by an endothermic RISC process for delayed fluorescence (DF). Consequently, 100% internal quantum yield can be expected by harvesting both singlet and triplet excitons in MR-TADF emitters.

To maximize the utilization of singlet and triplet excitons, a fast RISC process is necessary to avoid the exciton annihilation in other ways such as triplet-triplet annihilation (TTA) or singlet-triplet annihilation (STA).[61-63] Obviously, a small ΔE_{ST} is quite critical to speed up the RISC process according to the following Arrhenius equation 1:

$$k_{RISC} \propto \exp\left(\frac{-\Delta E_{ST}}{k_B T}\right) \qquad (1)$$

where k_B denotes the Boltzmann constant and T is the temperature.

Besides, the large SOC matrix element between singlet and triplet states can lead to relatively high rates of the endothermic RISC process which can also be computed according to the Fermi's golden rule (equation 2)[64, 65]:

$$k_{RISC} = \frac{2\pi}{\hbar}\rho_{FC} |< S_1 | H_{SOC} | T_1 >|^2 \qquad (2)$$

where $\langle S_1|\hat{H}_{SOC}|T_1\rangle$ denotes the SOC matrix element between the S_1 and T_1 states. ρ_{FC} represents the Franck-Condon-weighted density of states, which can be estimated according to the Marcus-Levich-Jortner theory. Therefore, reducing the ΔE_{ST} and enhancing the SOC are certainly critical to accelerate the RISC process, thereby improving the performance of MR-TADF-based OLED devices.[66]

2.1. Reducing the ΔE_{ST}

Generally, the energy level of S_1 is higher than that for T_1 by 0.5-1.0 eV in most organic molecules owing to the electron exchange energy between these levels.[67] To reduce the ΔE_{ST} of MR-TADF molecules, a special molecular design needs to be considered. In theory, the energies of S_1 (Es) and T_1 (E_T) are evaluated by the orbital energy (E), electron repulsion energy

(*K*) and exchange energy (*J*) of the two unpaired electrons at the excited states, as shown in the following equations 3-4:[18]

$$E_S = E + K + J \quad (3)$$

$$E_T = E + K - J \quad (4)$$

$$\Delta E_{ST} = E_S - E_T = 2J \quad (5)$$

Therefore, ΔE_{ST} which is the difference between E_S and E_T, is equal to the twice of *J* (equation 5). In other words, a small ΔE_{ST} value means that there is a minor overlap integral between the HOMO and LUMO.

The most widely adopted approach for separating the HOMO and LUMO distributions of the MR-TADF molecules is to enlarge the mixed degree of singlet and triplet states through peripheral modification or embedding heteroatom to the skeleton.[68-70] However, such a molecular design is adverse for the emission purity because it would usually cause the enlarged structure reorganization energy, resulting in an undesirable broad emission profile. In another way, extending the skeleton is beneficial for the enhanced molecular rigidity and reduced reorganization energy, thus realizing the narrowband emission. Furthermore, the theoretical and experimental investigations have demonstrated that the extension of MR framework can effectively reduce ΔE_{ST} and enlarge the oscillator strength concurrently based on the concept of charge transfer (CT) delocalization volume which shows a strong linear correlation (R^2 = 0.99) with ΔE_{ST}, with more extended skeletons the ΔE_{ST} is smaller and the oscillator strength is larger (**Figure 2a-c**)[71]. This result provides an unambiguous clue for designing high-performance MR-TADF emitters with both high emission efficiency and small ΔE_{ST}.

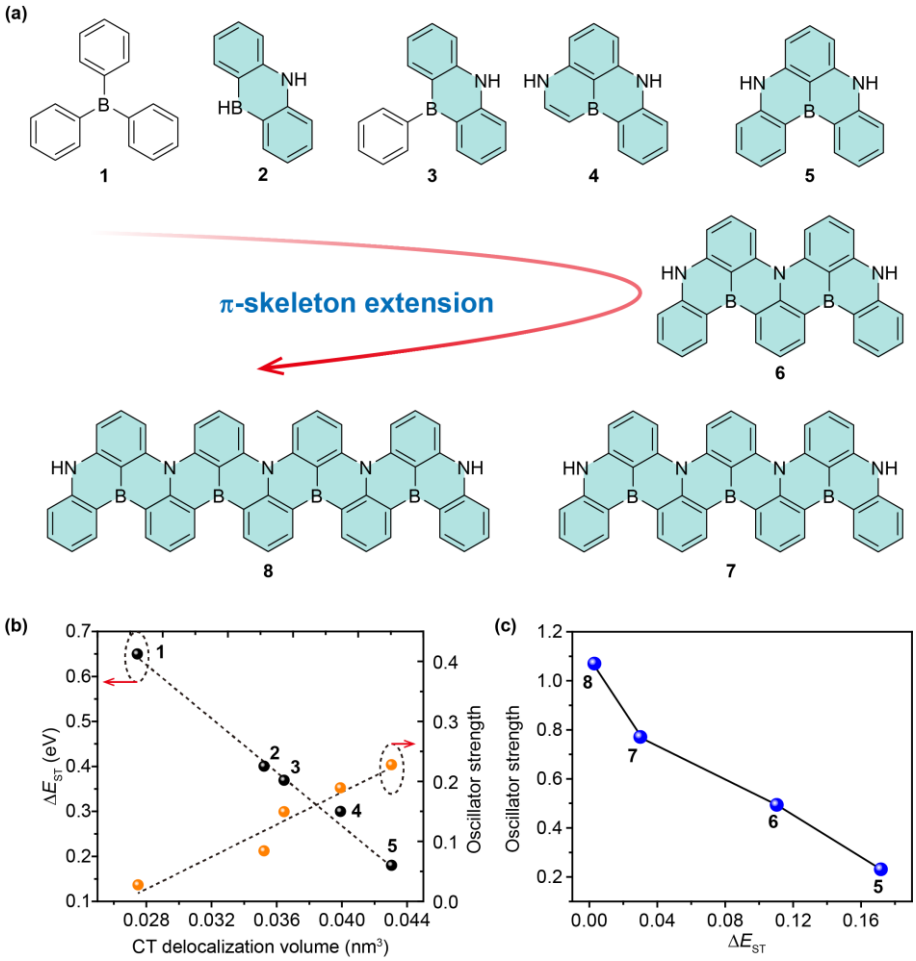

Figure 2. (a) Molecular structures involved with gradual extension of MR-skeleton. (b) ΔE_{ST} and oscillator strengths as a function of CT delocalization volume for the selected molecules **1-5**. (c) Oscillator strength as a function of ΔE_{ST} for molecules **5-8**.

2.2 Enhancing the SOC

SOC is a dominant force for driving the spin conversion and it can be enlarged significantly by regulating the electronic configurations of the singlet and triplet states.[72] According to the EI-Sayed rule,[73] considerable organic compounds show small SOC values (~10^{-1} cm^{-1}) and minor RISC rate constants (< 10^5 s^{-1}) because of the slow transitions between $^1(\pi, \pi^*)$ and $^3(\pi, \pi^*)$. By introducing heteroatoms (N, O, P, etc.) with lone-pair electrons, the S_1 of the MR-TADF molecules was endowed with dominant (n, π^*) characteristic while the T_1 keeping a mostly (π, π^*) feature. Thus, a large SOC constant was generated resulting from this large difference in the proportion of the n orbital (α_n) and π orbital (α_π) between S_1 and T_1 states (**Figure 3a**). Another common strategy to enhance the SOC matrix elements of MR-TADF emitters is to use heavy atoms (**Figure 3b**).[74, 75] Generally, the values of SOC are proportional to Z^4, where Z is the atomic nuclear charge. Therefore, introducing heavy atoms such as

chlorine (Cl), bromine (Br), iodine (I), sulfur (S) and selenium (Se) can easily induce a large SOC in MR-TADF molecules, thereby enabling the RISC rate constant to a higher level (> 10^5 s^{-1}).

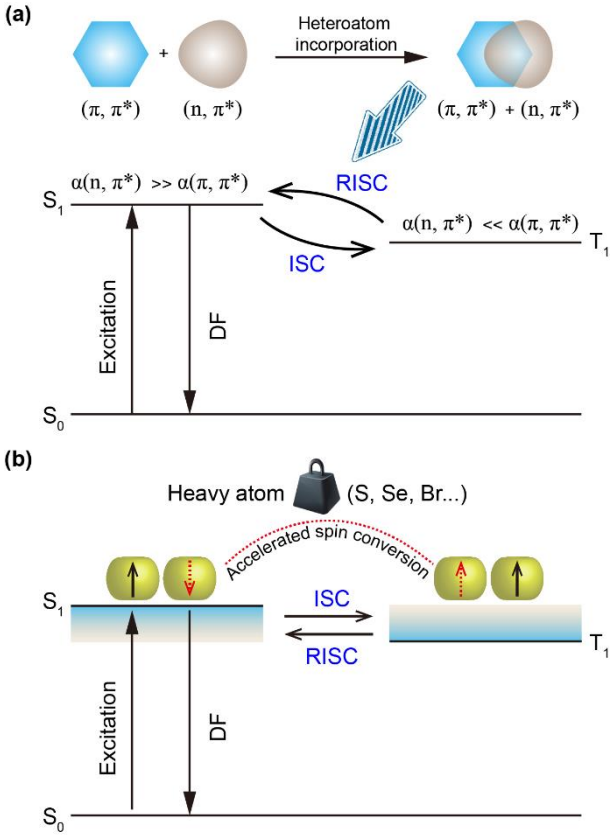

Figure 3. The strategies to accelerate the spin conversion by (a) introducing more (n, π*) characteristic to the singlet state via molecular engineering according to the EI-Sayed rule and (b) utilizing the heavy atom effect in the MR-TADF molecules.

3. Heavy-atom-integrated MR-TADF molecules

The spin-orbit perturbations of electronic states have a significant impact on the photophysical process of organic molecules. Integrating the heavy atoms into molecules leads to the enhancement of SOC matrix elements and the changes in photophysical parameters owing to the heavy-atom effect. This effect generally could be used as an effective strategy to achieve efficient TADF process with fast RISC rate.

3.1 Sulfur-containing MR-TADF emitters

Sulfur atom (S, Z_N = 16) as a “moderate” heavy atom can efficiently enhance the SOC to facilitate exciton spin-flipping for the facile RISC process with high rate constant, thereby shortening the lifetime of the DF component to prolong the work lifetime and suppress the efficiency roll-off of the devices. In recent years, considerable efforts have been made for

developing MR-TADF emitters based on the S atom (**Figure 4**). For example, Lu and co-workers designed and synthesized two green-emitting S-containing MR-TADF emitters **Cz-PTZ-BN** and **2Cz-PTZ-BN** by introducing the S atom into the MR-TADF B/N skeleton.[76] Because of the significantly enhanced SOC and asymmetrically peripheral protection, high photoluminescence quantum yields (PLQYs) of 91% and 96%, fast RISC rate constants of 0.81 × 10^5 and 1.05 × 10^5 s^{-1}, and short DF lifetimes of 20.7 and 17.6 μs were simultaneously realized for **Cz-PTZ-BN** and **2Cz-PTZ-BN**, respectively. It should be noted that **2Cz-PTZ-BN** showed higher PLQY and RISC rate than **Cz-PTZ-BN**, attributing to the peripheral modification of carbazole unit. Moreover, **Cz-PTZ-BN** and **2Cz-PTZ-BN** gave pure green emission with peaks at 510 and 505 nm, narrow FWHMs of 37 and 39 nm and small ΔE_{ST} values of 0.11 and 0.09 eV, respectively. As a result, the corresponding OLEDs displayed outstanding performance with the maximum EQEs of 26.6% and 32.8%, pure green EL emissions peaking at 520 and 516 nm with CIE coordinates of (0.26, 0.65) and (0.24, 0.63) for **Cz-PTZ-BN** and **2Cz-PTZ-BN**, respectively. Remarkably, the devices maintained high EQEs of 17.3% and 23.5% at the brightness of 1000 cd m^{-2}, demonstrating the suppressed efficiency roll-offs owing to the high RISC rate. In 2022, based on the similar asymmetrical peripherally protected concept, two classes of novel S-containing MR-TADF enantiomers **BN4** and **BN5** capable of TADF and circularly polarized luminescence (CPL) properties were developed by Chou et al.[77] Upon excitation, both **BN4** and **BN5** showed intense and narrowband emission with the maximum peaks at 500 and 497 nm and narrow FWHMs of 43 and 44 nm as well as high PLQYs of 88% and 87% in degassed toluene solution. Fast RISC processes with high rate constants of 1.6 × 10^5 and 7.4 × 10^4 s^{-1} and reduced delayed lifetimes of 8.3 and 23.1 μs for **BN4** and **BN5** were achieved because of the heavy atom effect of S atom. Furthermore, by introducing the dangling substituents of phenyl and methylene groups as the flexible lockers, solubilities of the MR TADF enantiomers can be increased which can be applied for the solution-processed OLEDs. Chiral enantiomers of **BN4**- and **BN5**-based OLEDs showed high performance with small FWHMs of 49/50 and 48/47 nm and high maximum EQEs of 20.6%/19.0% and 22.0%/26.5% as well as EL dissymmetry factor (g_{EL}) of +3.7 × 10^{-3}/-3.1 × 10^{-3} and +1.9 × 10^{-3}/-1.6 × 10^{-3}, respectively. These results demonstrate that the S atom could promote the performance of chiral MR-TADF materials. Furthermore, Yang and co-workers incorporated two sulfur atoms as the peripheral lockers into the MR polycyclic aromatic skeleton to construct a S-containing MR TADF molecule **2PTZBN**.[78] The emission peak was 510 nm with a small FWHM of 39 nm in solution, while the emission in doped film was red-shifted by 9 nm with a slightly enlarged FWHM of 44 nm. The more efficient RISC process with a high rate constant of 2.76 × 10^5 s^{-1}

and shortened delayed lifetime of 5.0 μs was realized in **2PTZBN**, resulting from the strong heavy-atom effect by two peripheral sulfur atoms. The OLEDs based on **2PTZBN** as the emitter showed a green EL emission with the peak at 527 nm and a small FWHM of 58 nm with the CIE coordinate of (0.28, 0.65) as well as high maximum EQE of 25.5%, maximum CE of 96.5 cd A^{-1} and maximum PE of 86.6 lm W^{-1}. Impressively, the EQE still remained as 21.7% and 17.2% at the luminance of 100 and 1000 cd m^{-2}, indicating low efficiency roll-offs of the **2-PTZBN**-based device benefited from the integration of S atom.

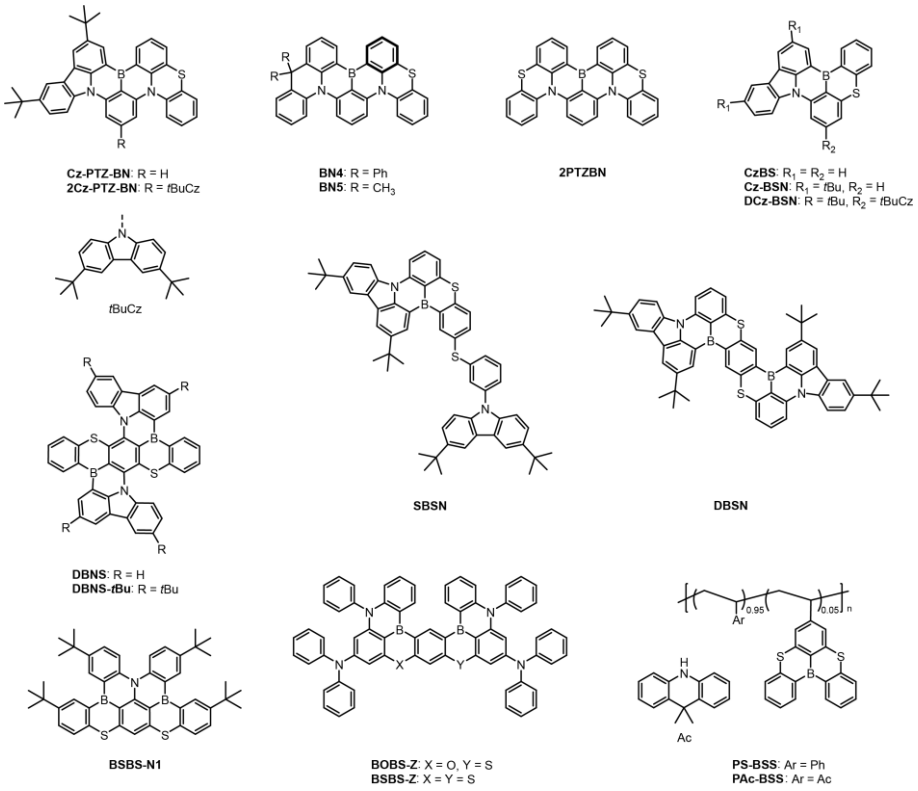

Figure 4. Molecular structures of sulfur-containing MR-TADF emitters.

Different from the above-mentioned peripheral locker, Yasuda et al. introduced the sulfur atom into the molecular skeleton to obtain a B/N/S-based S-containing MR TADF emitter **CzBS**.[79] The emission of **CzBS** was blue-shifted to 471 and 472 nm in solution and the 1 wt% doped film compared with the peripheral sulfur-locked molecules (> 500 nm). The FWHMs were 28 and 30 nm, and PLQYs were 99% and 98% in the solution and doped film states, respectively. An efficient RISC process with high RISC rate constants of 4.0×10^5 and 2.2×10^5 s^{-1} and shortened delayed lifetimes of 36 and 30 μs either in solution or film was observed, implying the important role of B/N/S structure. The **CzBS**-based OLED displayed a sky-blue emission with the maximum peak at 473 nm and a narrow FWHM of 31 nm, accompanied by high maximum EQE of 23.1%, maximum CE of 25.8 cd A^{-1}, and maximum PE of 19.4 lm W^{-1}. The EQEs still maintained at high values of 21.3% and 15.0% at 100 and 1000 cd m^{-2}. By

further adding two *tert*-butyl units into the 3- and 6-positions of carbazole group, the newly designed S-containing MR-TADF emitters **Cz-BSN** and **DCz-BSN** with a 3,6-di-*tert*-butylcarbazole unit in the *para*-position of B atom were reported by Wang et al.[80] The resultant N/B/S-doped MR emitters showed blue emission with the maximum peaks at 476 and 463 nm, narrow FWHMs of 24 and 26 nm, and high PLQYs of 82% and 88%, along with fast RISC rate constants of 0.96×10^5 and 1.04×10^5 s^{-1}, short delayed lifetimes of 40.8 and 49.1 μs for **Cz-BSN** and **DCz-BSN**, respectively, benefiting from the enhanced SOC values of 0.25 cm^{-1} (S_1-T_1) and 0.46 cm^{-1} (S_1-T_2) for **Cz-BSN**, and 0.30 cm^{-1} (S_1-T_1) and 0.43 cm^{-1} (S_1-T_2) for **DCz-BSN**. Consequently, efficient EL was achieved with the emission peaks at 482 and 473 nm, small FWHMs of 32 and 29 nm, and CIE coordinates of (0.11, 0.28) and (0.11, 0.17), together with maximum EQEs of 18.9% and 22.0% for **Cz-BSN** and **DCz-BSN**-based blue TADF devices, respectively.

By grafting a sulfur-containing π-conjugation moiety on the benzene of **Cz-BSN**, a ternary MR polycyclic aromatic emitter **SBSN** was developed and **DBSN** with *para* B-π-B and *para* S-π-S was also designed to further tune the photophysical properties for high-performance OLEDs with narrowband emission and small efficiency roll-off.[81] Impressively, **DBSN** showed a bathochromically shifted emission of 553 nm and high PLQY of 98% in doped film compared to those for **SBSN** (489 nm and 76%). Notably, both **SBSN** and **DBSN** possessed high RISC rates of 1.5×10^5 and 1.9×10^5 s^{-1}, and short delayed lifetimes of 32.2 and 25.7 μs in doped films, due to the small ΔE_{ST} values of 0.10 and 0.13 eV and the enhanced SOC values by introducing sulfur atoms. The blue and yellow OLEDs based on **SBSN** and **DBSN** displayed EL emission of 492 and 556 nm with the corresponding CIE coordinates of (0.10, 0.44) and (0.42, 0.57), together with the maximum EQEs of 26.7% and 21.8%, maximum CEs of 40.4 and 84.7 cd A^{-1}. Moreover, these devices exhibited low efficiency roll-off, where the EQEs remained at 12.0% and 16.9% at a practice luminance of 1000 cd m^{-2} for **SBSN** and **DBSN**-based devices, respectively. These excellent results were achieved primarily due to the high radiative rate and effective RISC process of sulfur doped **SBSN** and **DBSN**.

Subsequently, a kind of more rigid MR TADF emitters **DBNS** and **DBNS-*t*Bu** by integrating two pairs of S and N atoms and two B atoms in the *para*-positions of central benzene rings with a tridecacyclic aromatic framework were developed by Wang and co-workers.[82] Compared with the conventional B/N- and B/N/S-doped blue and green MR TADF emitters, the resultant emitters exhibited significant bathochromically-shifted emissions to the red region peaking at 631 and 641 nm with narrow FWHMs of 40 and 39 nm and high PLQYs of 80% and 85% in the solution states for **DBNS** and **DBNS-*t*Bu**, respectively, due to the strong ICT

enhanced by increasing the abilities of donor and acceptor in the *para*-arrayed B/N/S manner. Benefiting from the heavy-atom effect of S atom, the SOC values between the S_1 and T_n were significantly enhanced. Thus, the efficient RISC process with high rate constants of 2.1×10^5 and 2.2×10^5 s^{-1} and short DF lifetimes of 11.2 and 10.2 μs were obtained. Finally, by using **DBNS** and **DBNS-*t*Bu** as the emitters, the solution-processed red-emitting devices showed high performance with maximum CEs of 7.2 and 9.2 cd A^{-1} and maximum EQEs of 5.8% and 7.8% as well as narrow FWHMs of 66 and 65 nm (**Figure 5**). From this design, we can understand that sulfur atom allows the enhancement of the RISC rate constant of MR-TADF emitters.

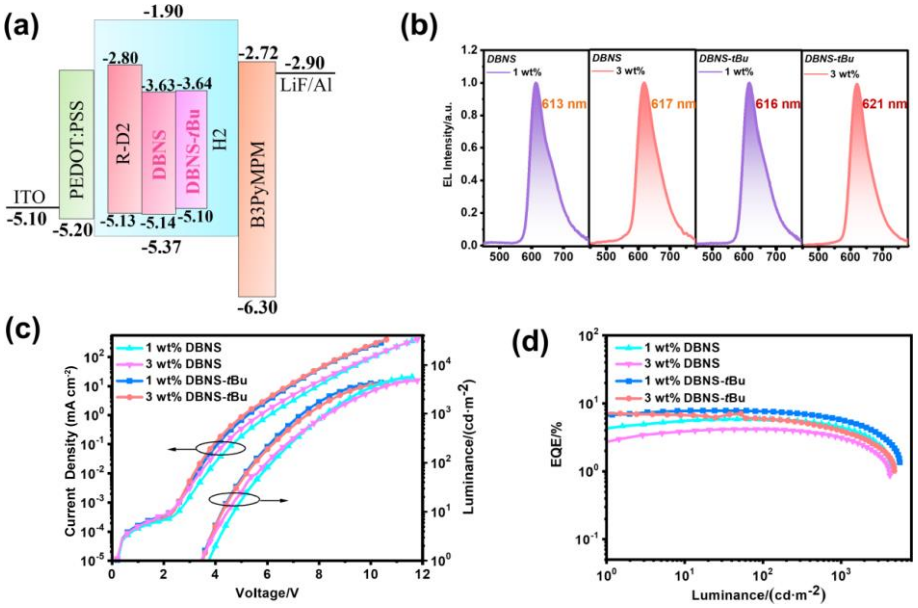

Figure 5. (a) Device configuration, (b) EL spectra with different doping concentrations, (c) current density-voltage-luminance characteristics, and (d) EQE versus luminance curves for **DBNS** and **DBNS-*t*Bu**-based solution-processed OLEDs. Reproduced with permission.[82] Copyright 2022, Wiley-VCH GmbH.

In 2021, Yasuda and co-workers proposed a ladder approach to construct fused-nonacyclic MR-TADF molecule **BSBS-N1** (**Figure 6**).[83] By strategically assembling with multiple B, N and S atoms, a narrowband sky-blue emission with a maximum peak at 478 nm, a small FWHM of 24 nm and a high PLQY of 89% was obtained for **BSBS-N1**. The ΔE_{ST} value of **BSBS-N1** was as small as 0.14 eV, and the large SOC values between S_1 and T_n (n = 1-4) ranged 0.31-1.51 cm^{-1}. Thus, the efficient RISC process with a high RISC rate constant of 1.9×10^6 s^{-1} and a short DF lifetime of 5.6 μs was achieved benefiting from the heavy-atom effect of S atom. Using **BSBS-N1** as emitter to fabricate OLED device achieved a narrow EL emission with a maximum peak at 478 nm and a narrow FWHM of 25 nm as well as a high maximum EQE of 21.0% and a suppressed efficiency roll-off. This work demonstrates that the integration of

"moderate" sulfur atom sheds light on the molecular design of highly efficient MR-TADF materials.

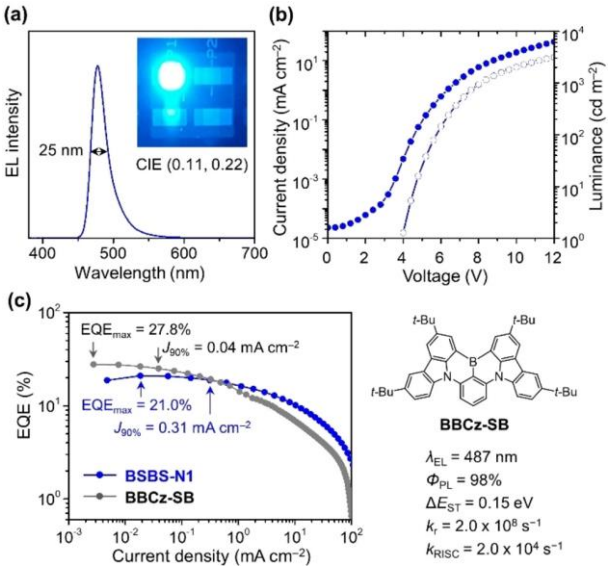

Figure 6. (a) EL spectrum and the corresponding EL photograph, (b) current density-voltage-luminance curves and (c) EQE versus current density plots of **BSBS-N1**-based OLED. In addition, the EQE curve of the **BBCz-SB**-based OLED fabricated with the same device condition was tested as a control device. Reproduced with permission.[83] Copyright 2021, Wiley-VCH GmbH.

Later, a series of fused polycyclo-heteraborin MR emitters **BOBS-Z** and **BSBS-Z** by exquisitely combining multiple B, N, O and S atoms were further developed by Yasuda's group.[84] The quaternary B/N/O/S-doped **BOBS-Z** and the ternary B/N/S-doped **BSBS-Z** exhibited narrowband blue emissions with the maximum peaks at 453 and 460 nm and narrow FWHMs of 21 and 20 nm. Compared with the B/N/O-doped MR counterpart (PLQY of 76%, k_{RISC} value of 7.0 × 10^4 s^{-1} and τ_{DF} of 7.7 μs), **BOBS-Z** and **BSBS-Z** afforded much higher PLQYs of up to 94%, faster k_{RISC} values as high as 8.6× 10^5 and 1.6 × 10^6 s^{-1}, and shorter lifetimes of 7.6 and 6.7 μs simultaneously, attributable to the heavy atom effect of the doped S atoms. The intense SOCs with the corresponding $\langle S_1|\hat{H}_{SOC}|T_n\rangle$ (n = 1-5) were in the range of 0.38-1.34 and 0.47-1.75 cm^{-1} for **BOBS-Z** and **BSBS-Z**, respectively. The OLEDs based on **BOBS-Z** and **BSBS-Z** gave blue EL spectra with the maximum peaks at 456 and 463 nm, narrow FWHMs as small as 23 and 22 nm, and CIE coordinates of (0.14, 0.06) and (0.13, 0.08), together with high maximum EQEs of 26.9% and 26.8%, maximum CEs of 16.7 and 23.2 cd A^{-1}, maximum PEs of 12.9 and 15.0 lm W^{-1}. Impressively, as the luminance was increased to 100 and 1000 cd m^{-2}, the EQEs were maintained at high values of 24.0% and 15.0% for the

BOBS-Z-based OLED and 24.0% and 15.9% for the **BSBS-Z**-based OLED, respectively, indicating the well-suppressed efficiency roll-offs due to their fast RISC processes.

Besides small molecules of sulfur-doped MR-TADF emitters, a new kind of narrowband blue MR-TADF polymers were designed and prepared by Wang et al. in 2021.[85] Based on the naphtho[3,2,1-*de*]anthracene polycyclic aromatic hydrocarbon framework, a B atom centered among three phenyl rings and two S atoms bridged over the phenyl rings were applied to construct the MR monomer **BSS**. Thanks to the enhancement of SOC by the heavy-atom effect from S atoms ($\langle S_1|\hat{H}_{SOC}|T_1\rangle$ of 0.77 cm^{-1} and $\langle S_1|\hat{H}_{SOC}|T_2\rangle$ of 0.32 cm^{-1} for **BSS**), the efficient RISC process with a fast rate constant of 1.18×10^5 s^{-1} and a short lifetime of 85.1 μs was realized for **BSS** monomer. For polymers, both **PS-BSS** and **PAc-BSS** showed narrowband emissions with the maximum peaks at 456 and 455 nm, small FWHM of 30 nm and PLQYs of 59%-60%. Moreover, the reduced lifetimes of 67.0 and 71.9 μs were observed for **PS-BSS** and **PAc-BSS** polymers compared with that for the BSS monomer. As a result, the solution-processed OLED by using **PAc-BSS** polymer as the emissive layer revealed a high-performance narrowband EL with the emission peak at 458 nm and a small FWHM of 31 nm as well as a promising device performance with the maximum CE of 17.7 cd A^{-1}, maximum PE of 13.0 lm W^{-1} and maximum EQE of 13.1%, respectively.

3.2 Selenium-containing MR-TADF emitters

The heavy atom effect of Se atom is more significant than that for S atom, thus the MR-TADF emitters integrating Se atom can achieve quite fast RISC process. Therefore, many Se-based MR-TADF molecules were proposed (**Figure 7**). Yasuda et al. firstly reported a blue MR-TADF emitter (**CzBSe**) doped with a heavier selenium atom (Se, $Z_N = 34$) based on the B/N/Se skeleton, realizing a record-high RISC rate constant as fast as 1.8×10^8 s^{-1}, which is more than three orders of magnitude higher than the typical values reported for MR-TADF emitters and even much higher than its fluorescence radiative rate (5×10^5 s^{-1}).[79] The theoretical simulations revealed that **CzBSe** has quite large SOC (5 cm^{-1} for $\langle S_1|\hat{H}_{SOC}|T_2\rangle$ and 10 cm^{-1} for $\langle S_1|\hat{H}_{SOC}|T_3\rangle$) values, which are larger than its O- and S-doped counterparts (CzBO and **CzBS**), demonstrating the remarkable heavy-atom effect of Se atom. As a result, the spin-flip process in **CzBSe** can be enlarged by ~20000 and ~800 folds compared to those for CzBO and **CzBS**, respectively. Consequently, **CzBSe**-based OLED showed a sharp sky-blue emission spectrum with the maximum peak at 481 nm and a narrow FWHM of 33 nm. Moreover, excellent device performance was achieved with high maximum EQE of 23.9%, maximum CE of 34.8 cd A^{-1} and maximum PE of 25.8 lm W^{-1}. Significantly, the **CzBSe**-based OLED achieved a quite small

efficiency roll-off, in which the EQEs remained at high values of 23.4% and 20.0% at 100 and 1000 cd m^{-2}, respectively. This work demonstrates that the Se-doped molecular design concept will promote the development of high-performance MR-TADF materials beyond the framework of traditional TADF molecules. Subsequently, by introducing additional *tert*-butyl and peripheral 3,6-di-*tert*-butylcarbazole moieties into the molecular framework of **CzBSe**, two selenium-integrated MR TADF emitters **Cz-BSeN** and **DCz-BSeN** were reported by Wang and co-workers in 2022.[86] These two compounds showed strong blue emissions with the maximum peaks at 479 and 472 nm in degassed toluene. Moreover, these two molecules showed smaller FWHMs of 30 and 28 nm than that for **CzBSe** (33 nm). It should be noted that the emission can be blue-shifted by 7 nm without widening the emission profile and the PLQY was enhanced to 93% in **DCz-BSeN** compared to those for **Cz-BSeN** owing to the peripheral modification of electron-donating carbazole unit. Significantly, these two emitters showed large SOC values (2.51 and 3.96 cm^{-1}) and high RISC rate constants of 7.5×10^6 and 8.8×10^6 s^{-1} for **Cz-BSeN** and **DCz-BSeN**, respectively, resulting from the heavy-atom effect of Se atom. The blue OLEDs containing 5 wt% **Cz-BSeN** and **DCz-BSeN** in the emissive layers gave narrowband EL emissions with maximum peaks at 490 and 481 nm and small FWHMs of 36 and 32 nm, together with maximum EQEs of 20.3% and 22.3%, maximum CEs of 44.0 and 32.3 cd A^{-1}, respectively. Impressively, these OLEDs achieved suppressed efficiency roll-offs with EQE values of 16.9-19.6% at 100 cd m^{-2} and 13.7-15.6% at 500 cd m^{-2}. This work revealed the potential of B, Se, N-doped MR-TADF molecules for the development of highly efficient narrowband blue devices with low efficiency roll-off.

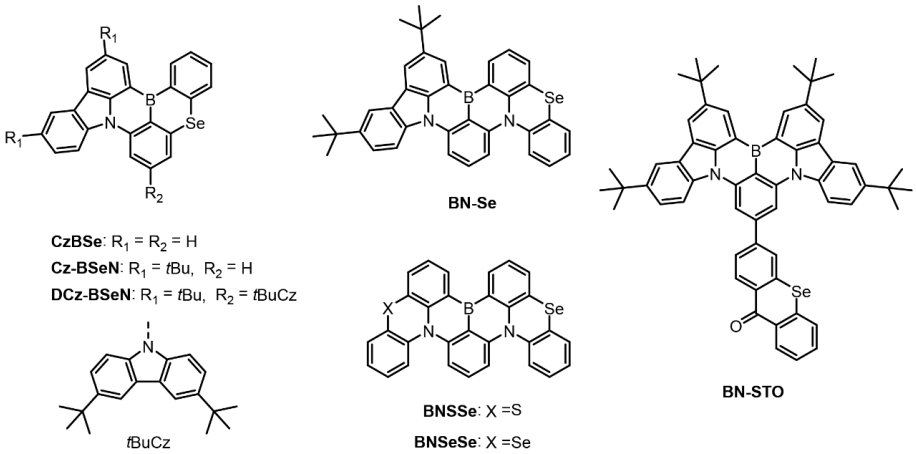

Figure 7. Molecular structures of selenium-containing MR-TADF emitters.

Compared to **CzBSe** and **Cz-BSeN**, a more extended selenium-embedded MR-TADF emitter **BN-Se** employing the 4,4'-diazaborin (N/B/N) skeleton was developed by Yang et al.[87] The extension of MR skeleton embedding the Se atom can make a small ΔE_{ST} and improved

emission efficiency for high-performance devices as well as a small reorganization energy. As expected, **BN-Se** exhibited an enhanced PLQY of 99%, a high RISC rate of 1.6×10^6 s^{-1} and a narrow emission profile with a maximum peak at 502 nm and a small FWHM of 42 nm. The OLED based on **BN-Se** as emitter exhibited outstanding EL performance with a small FWHM value of 45 nm, a maximum CE of 95.9 cd A^{-1}, a maximum PE of 103.9 lm W^{-1} and a maximum EQE of up to 32.6% without any outcoupling optimization. Impressively, this device achieved extremely low efficiency roll-off of 1.3% at 1000 cd m^{-2}. In order to realize faster RISC process, the same group proposed a double Se-integrated MR TADF emitter **BNSeSe** in the symmetric molecular structure to enhance SOC, and also developed an asymmetric molecule **BNSSe** for comparison.[48] As a result, due to the ultra-strong heavy atom effect of Se atom, an efficient RISC rate up to 2.0×10^6 s^{-1} for **BNSeSe** was achieved, while that of **BNSSe** was 6.0×10^5 s^{-1}. Both emitters showed green emissions with maximum peaks at 505 and 502 nm, small FWHMs of 39 and 38 nm, small ΔE_{ST} values of 0.12 and 0.14 eV and high PLQYs of 99% and 100% for **BNSSe** and **BNSeSe**, respectively. By using them as the emitters, excellent EL performances with high maximum EQEs, CEs and PEs of 35.7% and 36.8%, 124.2 and 121.0 cd A^{-1}, 156.2 and 146.3 lm W^{-1}, and extremely small efficiency roll-offs of 10.36% and 7.61% with EQEs of 32.0% and 34.0% at a high luminance of 1000 cd m^{-2} for **BNSSe** and **BNSeSe** were achieved (**Figure 8**). Furthermore, considering the high RISC rate constant of **BNSeSe** which was further employed as a sensitizer to sensitize the yellow-emitting MR-TADF molecules (BN3 and DtCzB-DPTRZ), the corresponding hyperfluorescence devices exhibited excellent maximum EQEs of 40.5% and 39.6%, and much suppressed efficiency roll-offs of 20.0% and 12.9% at a luminance of 1000 cd m^{-2}, respectively. These results clearly indicate that ultra-strong heavy atom effect of Se atom could efficiently accelerate the spin-flip process of MR-TADF emitters while keeping high emission efficiency and narrow emission profile, and thus further demonstrate the potential of MR-TADF emitters as sensitizers towards high-performance devices.

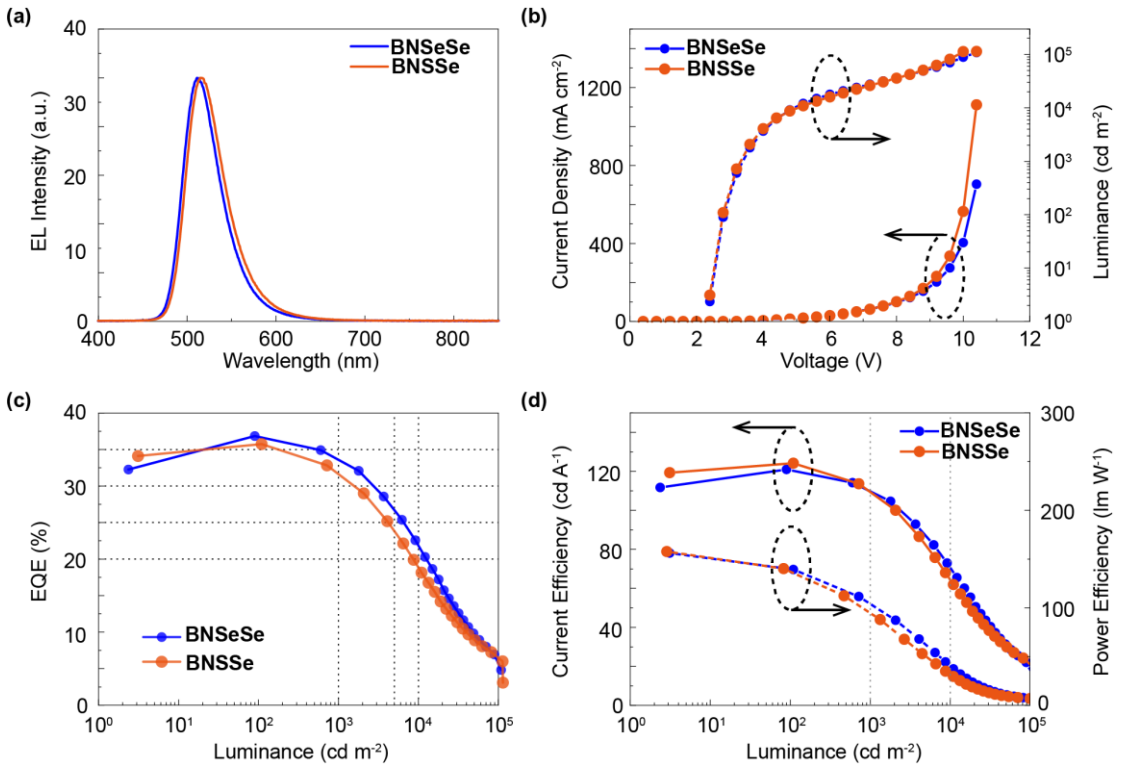

Figure 8. (a) Normalized EL spectra of the OLEDs based on **BNSSe** and **BNSeSe**, respectively. (b) Current density and luminance versus voltage curves, (c) EQE versus luminance characteristics and (d) current and power efficiency versus luminance curves of OLEDs based on **BNSSe** and **BNSeSe**, respectively.

The high performance of Se-integrated MR-TADF emitters was achieved, but Se atoms directly incorporated into MR skeleton usually leads to extended emission profile with high FWHM values, because of the large structural relaxation of phenoselenazine units with twist configurations upon the excitation-emission processes for the large reorganization energy. Therefore, Yang et al. proposed a novel design approach by peripherally introducing a selenium-embedded selenoxanthone unit which connected to the sky-blue MR-TADF unit BN-Cz to construct a Se-integrated MR-TADF emitter **BN-STO** to reach a balance between fast spin-flip process and narrow emission spectrum of MR-TADF molecules by the heavy atom effect.[88] As expected, **BN-STO** showed a green emission with a maximum peak at 506 nm and a small FWHM value of 29 nm. Moreover, a high RISC rate was obtained up to 1.2×10^5 s^{-1} owing to the strong SOC caused by the peripheral Se atom. The OLED device based on **BN-STO** showed an excellent performance with a high EQE of 40.1%, a high CE of 141.2 cd A^{-1} and a high PE of 176.9 lm W^{-1}. Remarkably, a much suppressed efficiency roll-off with high EQE near 30% at 1000 cd m^{-2} and a pure green EL emission with the CIE coordinate of (0.19, 0.70) were achieved. Furthermore, by introducing a TADF sensitizer 2,3,4,5,6-pentakis-(3,6-

di-*tert*-butyl-9H-carbazol-9-yl)benzonitrile (5TBuCzBN) to optimize the device performance of **BN-STO**, a maximum EQE of 38.4%, a maximum CE of 112.7 cd A^{-1} and a maximum PE of 137.6 lm W^{-1} were well achieved. Notably, in the hyperfluorescence OLED, the lower efficiency roll-off was realized and the EQE remained at 34.0% and 23.3% at 1000 and 5000 cd m^{-2}, respectively. These results demonstrate that the peripheral modification of heavy-atom for MR-TADF molecules is superior to the direct integration of heavy atom into the MR-TADF framework in terms of narrowing the emission profile.

3.3 The use of halogen

The introduction of halogens can improve the performance of OLEDs because of the significantly enhanced ISC and RISC processes. In 2022, Hong et al. firstly reported two MR TADF molecules **Cl-MR** and **Br-MR** by introducing halogen atoms (chlorine and bromine) into the *para* positions of three nitrogen atoms of an MR-TADF molecule, respectively (**Figure 9**).[89] These two emitters exhibited the same maximum emission peak at 460 nm and a small FWHM of 27 nm but **Cl-MR** showed a higher PLQY of 85% than **Br-MR** (76%). As expected, both **Cl-MR** and **Br-MR** exhibited increased RISC rates of 9.8×10^4 and 5.9×10^5 s^{-1}, significantly higher than that of 2.8×10^4 s^{-1} in the non-halogenated MR emitter. The short delayed lifetimes of 17 and 9.9 μs were observed for **Cl-MR** and **Br-MR**, respectively. Moreover, the better device performance with a high maximum EQE of 17%, a narrow FWHM of 30 nm and the CIE coordinate of (0.12, 0.19) was observed for **Cl-MR**-based OLED. Despite the significantly shortened delayed lifetime of **Br-MR**, its PLQY and device performance did not improve, which can be rationalized by the further analyses of kinetic rates and calculations of bond dissociation energy. These results suggested that the introduction of halogen atom could accelerate the RISC process, but the stability of MR-TADF emitters should be considered in the further development of high-performance OLEDs.

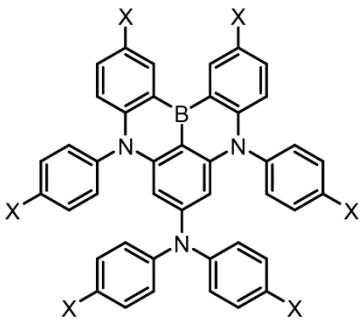

Cl-MR: X = Cl
Br-MR: X = Br

Figure 9. Molecular structures of halogen-containing MR-TADF emitters.

4. Metal-perturbed MR-TADF molecules

The strong SOC matrix elements are associated with the heavy atom, which could promote the exciton spin conversion. Besides the usual heavy atoms (S, Se), the metal atoms with higher atomic numbers, such as gold (Au) and platinum (Pt), can also significantly enhance the SOC for the rapid ISC and RISC processes. Moreover, the metal d orbital would give rise to a sub-microsecond delayed fluorescence lifetime when it is involved in the HOMO. This essential modification of excited state dynamics by introducing metal center demonstrates a feasible solution to boost the MR-TADF emission without reducing its color purity.

4.1 Gold(I) complex

Au(I), as one of the popular heavy metal atoms, would accelerate the ISC and RISC rates so that it can potentially shorten the emission lifetime for highly efficient TADF emission, because its d^{10} electronic configuration makes a minor contribution to excited state resulting in a large SOC constant of 5100 cm^{-1} between singlet and triplet excited states. In 2022, both the groups of Yang and Che demonstrated that the coordination of MR-TADF molecule with Au(I) atom via a C-deprotonated site can significantly speed up the RISC process from T_1 to S_1 excited state (**Figure 10**).[52, 90] The RISC rate of Au(I) MR-TADF emitter **DCzBN-Au** (**(SIPr)AuBN**) is up to 2.3×10^7 s^{-1}, which is greatly enlarged by 100-folds compared to that of the pure MR-TADF emitter DtBuCzB, attributing to the enhanced $\langle S_1|\hat{H}_{SOC}|T_1\rangle$ value of 0.21 cm^{-1} and the small ΔE_{ST} of 0.07 eV. In addition, **DCzBN-Au** showed a high PLQY of 88% and a small FWHM of 30 nm in the solution as well as the increased PLQY of 92% and slightly enlarged FWHM of 37 nm in the PMMA film. Furthermore, the vacuum-deposited OLED using **DCzBN-Au** as the emitter was fabricated, showing a high maximum EQE of 24.8%, a maximum CE of 86.1 cd A^{-1} and low EQE roll-offs of 2.0% and 18.9% at 1000 and 10000 cd m^{-2}, respectively (**Figure 11**). By changing the device configuration, a higher performance with a maximum EQE of 35.8%, a maximum CE of 112.5 cd A^{-1} and a maximum PE of 106.8 lm W^{-1} was achieved by Yang et al. This OLED showed a green EL emission of 510 nm with the corresponding CIE coordinate of (0.16, 0.67) and a narrow FWHM of 34 nm, and the EQE remained as high as 35.7% and 32.3% at 1000 and 10000 cd m^{-2}, displaying negligible efficiency roll-offs. The **(SIPr)AuBN**-based OLED also showed long operation lifetimes with LT_{90} and LT_{80} values of 73.4 and 150.1 h at an initial luminance of 1000 cd m^{-2}. Moreover, due to the increased solubility by the pendant ancillary carbene ligand of Au ion, the solution-processed OLED was also fabricated by using **(SIPr)AuBN** as the emitter. The EL emission peaking at 510 nm and the CIE coordinate of (0.18, 0.67) were observed, which were very close

to those of the vacuum-deposited device. Specially, the solution-processed OLED exhibited a high maximum CE of 84.0 cd A^{-1}, a maximum PE of 75.4 lm W^{-1} and a maximum EQE of 25.7%. Moreover, the EQEs of **(SIPr)AuBN**-based devices still maintain high values of 23.5% and 11.7% at 1000 and 10000 cd m^{-2}, respectively. These data indicate that the metal-coordinated MR-TADF emitters can improve the device performance and realize small efficiency roll-off owing to the fast RISC rate.

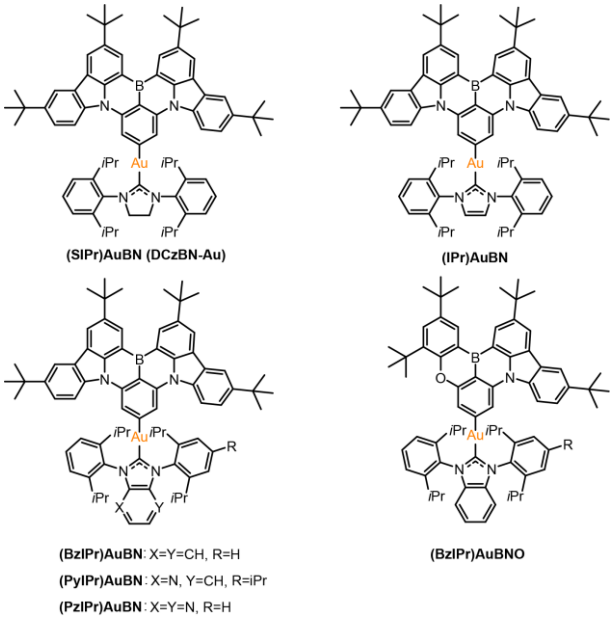

Figure 10. Molecular structures of metal-containing MR-TADF emitters.

By changing the nitrogen-substituted ancillary ligand, a series of efficient Au(I) MR TADF emitters **(IPr)AuBN**, **(BzIPr)AuBN**, **(PyIPr)AuBN**, **(PzIPr)AuBN** based on the N/B/N MR-TADF skeleton were developed, and another Au(I) MR-TADF emitter **(BzIPr)AuBNO** employing the newly prepared MR-TADF molecule containing the N/B/O unit was also designed and synthesized.[90] As expected, all the emitters afforded bright green emissions with the maximum peaks at around 510 nm and narrow FWHMs as small as 30 nm as well as high PLQYs in the range of 78%-93%, except that the emission of **(BzIPr)AuBNO** was obviously blue-shifted to 471 nm. Benefiting from the effect of Au(I) coordination, the fast RISC rates were obtained, being around 10^6 s^{-1}, which were significantly enlarged by about 30- to 170-fold compared to those for metal-free B/N- and B/N/O-based MR-TADF emitters, respectively, and consequently their DF lifetimes were notably reduced to 5.5-27.0 μs in a mono-exponential function. Therefore, the OLEDs based on these Au(I) MR-TADF emitters showed high performance with sharp green EL emissions peaking at 508-517 nm and small FWHMs of 34-40 nm. Impressively, these devices exhibited high EQEs of up to 30.3% combined with high CE of 97.1 cd A^{-1}, which were much higher than those for the pure B/N- based devices (EQE

of 13.6% and CE of 28.5 cd A^{-1}). Moreover, due to the shortened triplet exciton lifetimes, the Au(I) MR-TADF emitter-based OLEDs displayed suppressed efficiency roll-offs of 0.8%-6.0%, and long operational lifetime (LT_{60}) of 1210 h at a practical luminance of 1000 cd m^{-2}. These molecular design of metal-perturbed MR-TADF emitters can significantly promote triplet exciton harvesting, thereby realizing high-performance MR-TADF OLEDs and opening up a new dimension to design practical MR-TADF emitters.

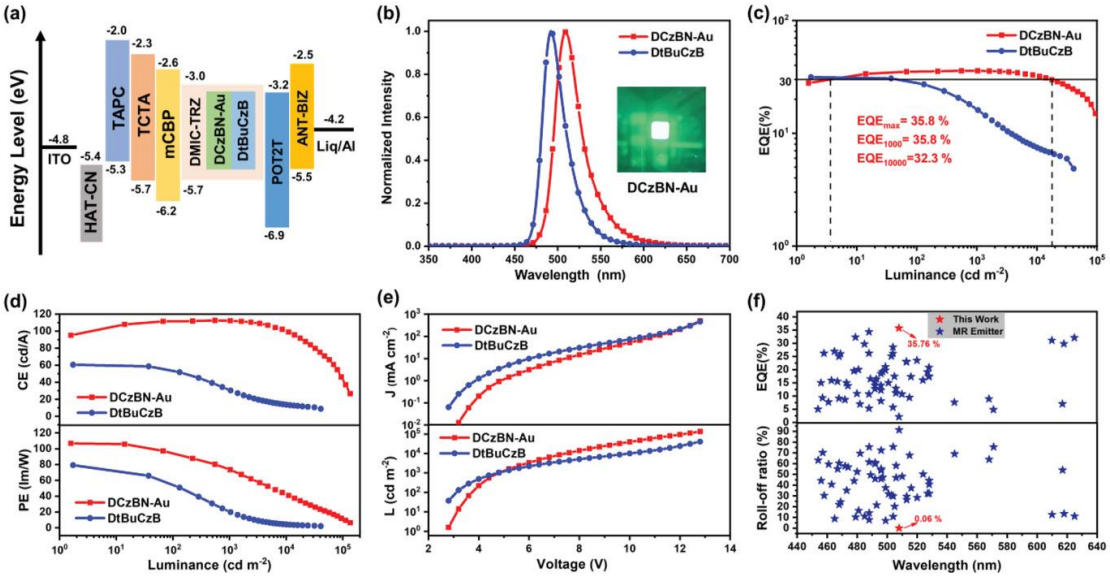

Figure 11. (a) The OLED structure and energy diagram of the involved materials. (b) EL spectra of devices at 1000 cd m^{-2}, and inset shows the EL photograph of the device based on **DCzBN-Au**. (c) EQE versus luminance characteristics, (d) current and power efficiency versus luminance characteristics and (e) current density and luminance versus voltage curves of the devices based on **DCzBN-Au** and DtBuCzB. (f) Summary of the maximum EQEs and roll-offs at 1000 cd m^{-2} versus wavelength. Reproduced with permission.[52] Copyright 2022, Wiley-VCH GmbH.

4.2 Platinum(II) complex

Recently, Wang et al. reported a feasible molecular design strategy to construct a desirable MR platinum(II) complex **BNCPPt** by integrating an original MR TADF unit into the classical heavy metal platinum(II) complex (**Figure 12**).[91] This complex showed a remarkable light green emission with a maximum peak at 497 nm and a small FWHM of 27 nm in toluene, while it exhibited a slight red shift and a widened FWHM in the doped film because of the aggregation of dopant in the solid state. Impressively, because of the heavy platinum(II) ion, the $\langle T_2|\hat{H}_{SOC}|S_0\rangle$ value for **BNCPPt** is as large as 258.99 cm^{-1}, with a short emission lifetime of 3.78 μs. These excellent properties of **BNCPPt** have tremendous advantage for achieving

promising OLED devices. This design concept provides an ingenious combination of MR unit and phosphorescent metal complexes, demonstrating a novel strategy to construct the phosphorescent complexes with high emission purity towards high-performance EL devices.

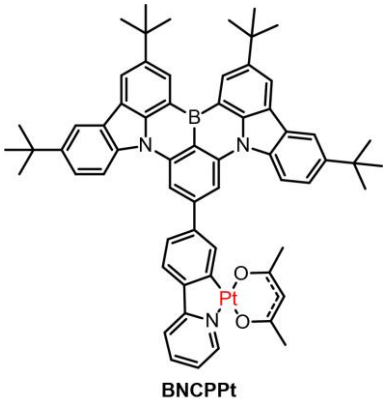

Figure 12. Molecular structure of platinum-containing MR-TADF emitter.

5. π-skeleton extended MR-TADF molecules

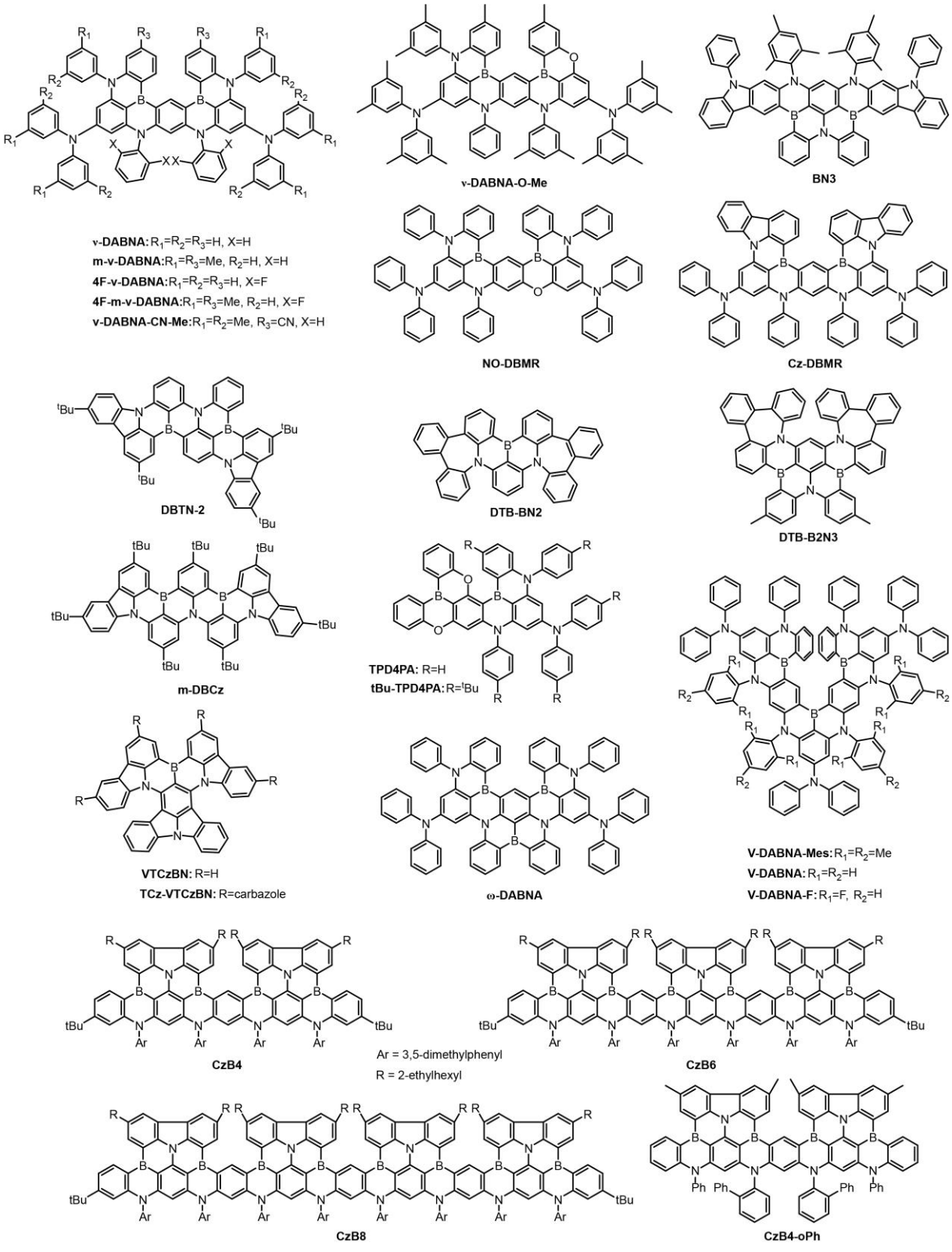

Figure 13. Molecular structures of π-skeleton extended MR-TADF emitters.

In 2019, Hatakeyama and co-workers developed a novel MR-TADF emitter **ν-DABNA** with an extended π-skeleton, in which five benzene rings were linked by two B and four N atoms

(**Figure 13**).[32] In this design strategy, the electron-withdrawing B atom is surrounded by electron-donating nitrogen atoms at the *para*-position, such MR effect can well separate the distributions of HOMO and LUMO and even minimize the bonding/antibonding character and the vibronic coupling between the S_0 and S_1 states as well as the vibrational relaxation at the S_1 state. Therefore, a small ΔE_{ST} of 17 meV and an extremely narrow emission spectrum with a FWHM of 14 nm were observed in the doped film. With such a small ΔE_{ST}, the efficient TADF properties were obtained with a fast RISC rate of 2.0×10^5 s^{-1}, which is much higher than the traditional MR-TADF molecules with simple MR unit. The device by using **ν-DABNA** as dopant realized an excellent performance with a pure blue emission peaking at 469 nm and an extremely narrow FWHM of 18 nm which is even narrower than those of the quantum dot LEDs. Furthermore, this OLED gave a maximum EQE of 34.4%, 32.8% at 100 cd m^{-2} and 26.0% at 1000 cd m^{-2} (**Figure 14**). Impressively, the efficiency roll-off (1.6% and 8.6% at 100 and 1000 cd m^{-2}, respectively) is lower than those for most of the reported deep-blue OLEDs owing to the fast RISC process which can significantly suppress the TTA and STA processes in the EL process. However, the CIE *y* coordinate of the **ν-DABNA**-based device is 0.11, which hardly satisfies the pure blue color requirements of the Broadcast Service Television 2020 (BT2020).

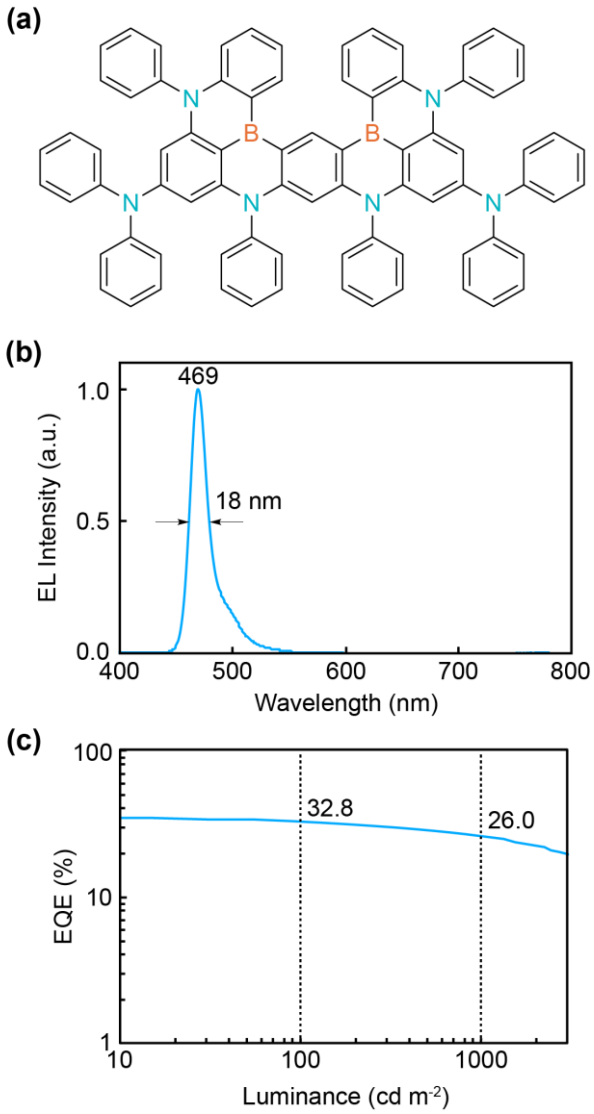

Figure 14. (a) Molecular structures of **ν-DABNA**. (b) EL spectrum. (c) EQE versus luminance curve.

Since the report of **ν-DABNA**, tremendous efforts have been devoted to modify the molecular structure for achieving deep blue or green emission and further facilitating the RISC process. Based on the modification of **ν-DABNA**, Naveen et al. introduced the fluorine atoms and methyl units and thus synthesized three deep-blue emitters, **m-ν-DABNA**, **4F-ν-DABNA**, and **4F-m-ν-DABNA**.[92] Introducing the methyl groups into the *para* positions of the electron-withdrawing B atoms and fluorine atoms into the *ortho* positions of the electron-donating nitrogen atoms can efficiently increase the bandgap for the blue-shifted emission spectra. As expected, all these three molecules showed deep-blue emissions with high PLQYs up to 90%, small ΔE_{ST} ($\leq$ 0.07 eV) values and high RISC rate constants up to 2.3×10^5 s^{-1} which is slightly higher than that for **ν-DABNA** (2.0×10^5 s^{-1}), indicating their highly efficient TADF properties. All fabricated OLEDs by using DBFPO as a host showed the emission peaks in the range of

461-471 nm, along with narrow FWHM values of only 18 nm owing to the rigid molecular skeleton, thereby realizing the deep-blue color with the CIE coordinates of (0.12, 0.12), (0.13, 0.08) and (0.13, 0.06) for **m-ν-DABNA**-, **4F-ν-DABNA**- and **4F-m-ν-DABNA**-based OLEDs, respectively. Impressively, the OLEDs realized maximum EQE of 36.2%, 35.8% and 33.7% for **m-ν-DABNA**-, **4F-ν-DABNA**- and **4F-m-ν-DABNA**, respectively, and all of the OLEDs showed extremely low efficiency roll-offs owing to the fast RISC rate. Moreover, Hatakeyama et al. reported a cyano-substituent **ν-DABNA** (**ν-DABNA-CN-Me**) via a one-shot double borylation and palladium-catalyzed cyanation protocol, resulting in a remarkable bathochromic shift compared to **ν-DABNA** without broadening the emission profile.[93] **ν-DABNA-CN-Me** exhibited a pure green TADF emission peaking at 508 nm and a narrow FWHM of 17 nm as well as a high RISC rate constant of 10^5 s^{-1} in toluene solution. The **ν-DABNA-CN-Me** based device exhibited excellent performance with EQE values of 31.9%, 31.5% and 28.5% at 10, 100, and 1000 cd m^{-2}, respectively. In addition, the efficiency roll-offs of the OLED based on **ν-DABNA-CN-Me** (0.4 and 3.4% at 100 and 1000 cd m^{-2}, respectively) were lower than the those in the most reported green OLEDs based on the MR-TADF emitters.

In addition, Hatakeyama et al. also developed a strategy to shift the emission of **ν-DABNA** to deep-blue color by replacing a nitrogen atom with an oxygen atom which has a lower atomic orbital energy and a weaker electron-donating ability compared to the nitrogen atom.[94] The resultant **ν-DABNA-OMe** exhibited a blue-shifted emission spectrum and a comparable RISC rate constant of 1.6×10^5 s^{-1} to that for **ν-DABNA** (2.0×10^5 s^{-1}), even though the FWHM was increased to 19 nm, ΔE_{ST} was risen to 29 meV. The OLEDs were fabricated using 1 wt% **ν-DABNA-OMe** as dopant, demonstrating a high performance with a pure blue emission peaking at 464 nm and a narrow FWHM of 24 nm as well as a maximum EQE of 29.5%. Significantly, **ν-DABNA-OMe** showed a much reduced efficiency roll-off of only 2.6% at 1000 cd m^{-2} compared to that for **ν-DABNA** (8.4%) probably owing to the suppressed bimolecular quenching process such as TTA and TPA.

In order to reveal the effect of π-extension on the photophysical and EL behaviors, Yang et al. developed a kind of narrowband deep-blue MR-TADF molecules (**BN1**-**BN3**) with gradually extended MR-skeleton (**Figure 15**).[95] These compounds were obtained from the same precursor by lithium-free borylation in high yields at optimized conditions. All these three molecules showed narrow deep-blue emission spectra with FWHMs of less than 18 nm and significantly small ΔE_{ST} values ≤ 0.20 eV in toluene solution owing to the rigid and extended molecular skeleton. Specifically, **BN3** showed the highest PLQY of 98% and the fastest RISC rate constant of 2.55×10^5 s^{-1} among them. Therefore, **BN3**-based deep-blue OLED realized

the highest EQE value of 37.6% and the smallest efficiency roll-off because of the much accelerated RISC process, demonstrating the effectiveness of the π-extension method to improve the RISC process and enhance the device performance for MR-TADF emitters.

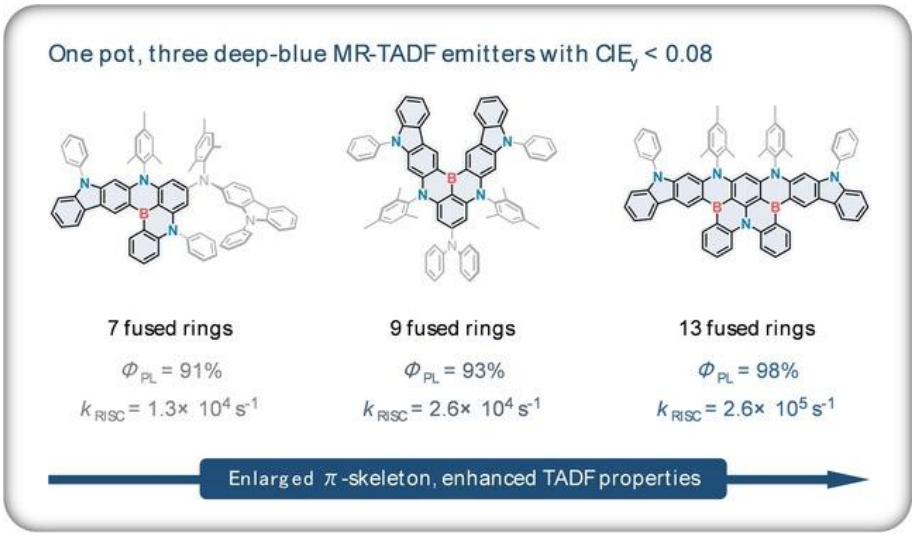

Figure 15. Three boron/nitrogen-based deep-blue molecules of **BN1**, **BN2** and **BN3** with gradually extended π-skeleton. Reproduced with permission.[95] Copyright 2022, Wiley-VCH GmbH.

Recently, Kwon et al. reported two molecules (**NO-DBMR** and **Cz-DBMR**) to show hypsochromic and bathochromic shifts of **ν-DABNA** emission by introducing the oxygen and carbazole moieties.[96] **NO-DBMR** contains an unsymmetric structure containing both O-B-N and N-B-N units. **Cz-DBMR** forms the symmetrical core with carbazole moiety, which can enhance the rigidity of the skeleton for narrowing the emission profile. These two molecules showed pure blue, bluish-green emission with the same extremely narrow FWHM of 14 nm and small ΔE_{ST} (40 meV) as well as high PLQYs of over 80%. Moreover, fast RISC rate constants of **NO-DBMR** (1.04×10^5 s^{-1}) and **Cz-DBMR** (3.72×10^5 s^{-1}) were observed owing to the short delayed lifetimes. Therefore, the fabricated OLEDs based on **NO-DBMR** and **Cz-DBMR** manifested the excellent performance with maximum EQE of 33.7% and 29.8%, respectively.

To further enhance the SOC, Zhang et al. proposed a novel molecular design strategy by distorting fused π-extended structure. A B/N-based MR-TADF molecule **DBTN-2** was synthesized by introducing multiple carbazole moieties.[97] Due to its highly distorted fused π-conjugated framework, the excitation characters of the S_1 (ππ* excitation) and T_1/T_2 (hybrid excitation of ππ* and πσ*) states are different, contributing to the enhanced SOC between the singlet and triplet excited states according to the EI-Sayed rule. Moreover, the introduction of

multiple carbazole groups results in a charge-resonance-type excitation feature of the T_1 and T_2 states. As a result, the reduced T_1-T_2 energy gap and thus accelerated $T_2 \rightarrow S_1$ up-conversion channel were expected. Therefore, the large SOC matrix element of 0.46 cm^{-1} and fast RISC rate constant of 1.7×10^5 s^{-1} were achieved in **DBTN-2**. Finally, the **DBTN-2**-based OLED was fabricated, exhibiting a pure green emission peaking at 520 nm and a narrow FWHM of 29 nm as well as a maximum EQE of 35.2% and a suppressed efficiency roll-off (33.6% at 100 cd m^{-2} and 20.4% at 1000 cd m^{-2}) owing to the reduction of triplet-related annihilation processes induced by the fast RISC process. In addition, You et al. proposed a medium-ring molecular design strategy, intending to concurrently increase the RISC rate constant and suppress aggregation-caused quenching effect of MR-TADF molecules for the improved efficiency roll-off of the OLEDs based on the MR-TADF emitters (**Figure 16**).[98] The designed MR-TADF emitters (**DTBA-BN2** and **DTBA-B2N3**) feature two highly twisted heptagonal tribenzo[*b*,*d*,*f*]azepine donors, resulting in increased intermolecular distances between the MR units as well as suppressed π-π interactions. More importantly, introducing the heptagonal donor enables us to increase the SOC matrix elements, thereby giving rise to a fast RISC rate of 2.3×10^5 and 1.6×10^6 s^{-1} for **DTBA-BN2** and **DTBA-B2N3**, respectively. Finally, the OLEDs were constructed by using **DTBA-BN2** and **DTBA-B2N3** as the emitters and 26DCzPPy as the host. The 3 wt% doped **DTBA-BN2** and **DTBA-B2N3**-based devices showed the best EL performance with maximum EQE values of 31.2% and 30.9% and the EQE values of 25.6% and 20.5% at the luminance of 1000 cd m^{-2}, respectively. This outstanding performance is among the best results of reported MR-TADF OLEDs.

Figure 16. The medium-ring molecular design strategy for high-performance MR-TADF emitters with fast spin-flip to suppress efficiency roll-off. Reproduced with permission.[97] Copyright 2023, Wiley-VCH GmbH.

To simultaneously realize the red-shifted emission and short delayed fluorescence lifetime, Wang et al. reported a molecule (***m*-DBCz**) by assembling MR-building blocks to form a more extended and rigid molecular configuration.[99] The appropriately covalent bond connection and

geometric arrangement of MR building blocks would result in a high-efficiency narrowband emission within the longer wavelength region and short delayed fluorescence lifetime. Thus, ***m*-DBCz** exhibited excellent photophysical properties with a narrowband yellowish-green emission peaking at 541 nm, a small FWHM of 32 nm and a high PLQY of 95% as well as a fast RISC rate constant of 1.5×10^5 s^{-1}. The OLED using ***m*-DBCz** as the emitter showed an emission peak at 548 nm and a small FWHM value of 35 nm, as well as a maximum EQE of 34.9%. The EQEs remained to be 31.3% at 1000 cd m^{-2}, 24.5% at 5000 cd m^{-2} and 20.0% at 10000 cd m^{-2}. The small efficiency roff-off is originated from its fast RISC rate.

Extending the π-skeleton of MR-TADF emitters by integrating different MR units can efficiently regulate the photophysical and electroluminescence performance of MR-TADF emitters. On the basis of this idea, Kwon et al. developed two deep blue MR-TADF emitters (**TPD4PA** and **tBu-TPD4PA**) by the fusion of O-B-O and N-B-N MR groups into one molecule.[100] Both emitters showed the deep blue emission with the maximum peaks at 445 (**TPD4PA**) and 451 nm (**tBu-TPD4PA**) and a small FWHM value of 19 nm in toluene solution. Importantly, the small ΔE_{ST} values of 0.05 and 0.06 eV for **TPD4PA** and **tBu-TPD4PA** are also reserved in this molecular design, supporting for a large RISC rate constant of 2.51×10^5 s^{-1}. The OLEDs fabricated by using **TPD4PA** and **tBu-TPD4PA** as the emitters displayed the maximum EQEs of 30.7% and 32.5% and the EQE values still maintained at 30.6% and 30.9% at the luminance of 100 cd m^{-2}. Besides, Zheng and co-workers designed two MR-TADF emitters **VTCzBN** and **TCz-VTCzBN** based on the fusion of indolo[3,2,1-jk]carbazole and N/B/N dual component resonant skeletons.[70] As expected, these two emitters displayed small ΔE_{ST} values of 0.06 and < 0.01 eV for **VTCzBN** and **TCz-VTCzBN**, respectively, due to the enhanced MR effect by hybridizing dual-component fused MR units. Moreover, large SOC matrix elements of 0.154 and 0.286 cm^{-1} were realized without the introduction of heavy atoms. Consequently, the fast RISC rate constants of 1.0×10^6 and 0.9×10^6 s^{-1} can be obtained for **TCzBN** and **TCz-VTCzBN**, respectively. Therefore, **VTCzBN**- and **TCz-VTCzBN**-based devices gave the maximum EQEs of 31.7% and 32.2% and the EQEs of 24.8% and 18.0% at the luminance of 100 cd m^{-2}, respectively. These reports demonstrate that the extension of typical N-B-N MR framework by integrating different MR unit would be an alternative way to construct the high-performance MR-TADF emitters.

Indeed, extending the π-skeleton can reduce the ΔE_{ST} and thus accelerate the RISC rate. To further extend the π-skeleton of MR-TADF emitters, the compounds containing three boron atoms for multiple MR units were explored. For example, Hatakeyama et al. developed an expanded heterohelicene **V-DABNA-Mes** by using three BN2-embedded [4]helicene subunits

through one-shot borylation.[101] The special synthesis for **V-DABNA-Mes** is to use the excessive boron tribromide in an autoclave. Benefiting from the rigid molecular skeleton and accumulated MR effect, **V-DABNA-Mes** afforded an extremely narrow emission profile with a small FWHM of 16 nm in the doped film and a minimized ΔE_{ST} to 5.2 meV as well as a triggered rapid RISC process with a rate constant of 4.4×10^5 s^{-1} which is two times higher than that for **ν-DABNA** (2.0×10^5 s^{-1}). The solution-processed device based on **V-DABNA-Mes** as the dopant showed an emission peak at 480 nm with a narrow FWHM value of 27 nm, and realized a maximum EQE of 22.9% and remained a high EQE of 20.3% at the luminance of 100 cd m^{-2}. However, there is an awkward problem that the molecular weight of **V-DABNA-Mes** is too high to fabricate the OLED by vapor deposition. Later, they further synthesized **V-DABNA** and a fluorine-substituted derivative (**V-DABNA-F**) with significantly reduced molecular weight which can be processed with vapor deposition.[102] By the study of photophysical properties, **V-DABNA-F** revealed an ultrapure blue emission profile with a narrow FWHM of 16 nm. Moreover, the small ΔE_{ST} values of 6.0 and 4.9 meV were figured out for **V-DABNA** and **V-DABNA-F**, respectively. With such a small ΔE_{ST}, the fast RISC process would be expected for **V-DABNA** (5.7×10^5 s^{-1}) and **V-DABNA-F** (6.5×10^5 s^{-1}), respectively. The blue OLED eventually fabricated by using **V-DABNA** as a dopant by vapor deposition displayed a sharp emission profile with a maximum peak at 483 nm and a narrow FWHM of 17 nm. Moreover, outstanding performance with high EQEs of 26.2%, 26.2%, and 25.3% at 1, 100 and 1000 cd m^{-2} was achieved, respectively. Impressively, this OLED showed good stability with the half-lifetime (LT_{50}) of 184 h at an initial luminance of 500 cd m^{-2}, which is much longer than that for ***ν*-DABNA**-based device (2 h at an initial luminance at 500 cd m^{-2}) because of the fast RISC rate. Besides, the **V-DABNA-F**-based OLED showed an ultrapure deep-blue emission with the maximum peak at 468 nm and a narrow FWHM of 15 nm. Meanwhile, a high maximum EQE of 26.6% was realized with a quite small efficiency roll-off (25.8% and 23.4% at 100 and 1000 cd m^{-2}, respectively) benefitting from the accelerated RISC process. Very recently, the same group proposed a sequential multiple borylation reaction including one-pot borylation, amination, and one-shot borylation to further explore the chemical space remained in the MR-TADF molecules. Therefore, an ultrapure green MR-TADF molecule **ω-DABNA** was designed and synthesized consisting of multiple B and N atoms (**Figure 17**).[103] With an extended MR skeleton and rigid molecular framework, **ω-DABNA** showed an extremely sharp green emission peaking at 509 nm with a narrow FWHM of 22 nm as well as a small ΔE_{ST} of 13 meV, thus the short delayed lifetime of 8.95 μs and the high RISC rate constant of 1.5×10^5 s^{-1} were estimated. The OLED by using **ω-DABNA** as the

emitter gave an emission at 512 nm with a small FWHM value of 25 nm. Moreover, an excellent OLED performance was achieved with a high maximum EQE of 31.1% and much suppressed efficiency roll-off (only 1.4% at 1000 cd m^{-2}) owing to the high PLQY of 87% and fast RISC process. These design concepts clearly show that integrating multiple MR units into one rigid molecular skeleton can facilitate the RISC process and alleviate the efficiency roll-off for achieving excellent device performance.

Impressively, Hatakeyama et al. constructed a kind of MR-TADF molecules with BN-embedded nonacene (**CzB4**), tridecacene (**CzB6**), and heptadecacene (**CzB8**) frameworks by one-shot quadruple, sextuple, and octuple borylation reactions, which are the largest MR-TADF core structures reported so far.[104] These molecules exhibited extremely narrow green TADF emission with a small FWHM of 12-16 nm and high PLQY of 0.92-0.94. Moreover, the distributions of HOMO and LUMO are located at large acene skeleton, resulting in a small ΔE_{ST}. With the framework expansion from **CzB4** to **CzB8**, the ΔE_{ST} is reduced from 4.2 to 3.0 meV and the RISC rate is increased from 1.8×10^5 to 6.5×10^5 s^{-1}. These three molecules cannot be fabricated into the OLEDs by vapor deposition owing to their large molecular weight. To demonstrate the potential of the **CzBn** series as emitters for OLEDs, the authors synthesized a new nonacene derivative (**CzB4-oPh**) to characterize the device performance. The OLED based on **CzB4-oPh** showed the emission peak at 490 nm and a small FWHM of 21 nm. Significantly, the fabricated OLED showed a high maximum EQE of 28.7% and a quite small efficiency roll-off (2.9% at 1000 cd m^{-2}), which were attributed to its high PLQY and high RISC rate.

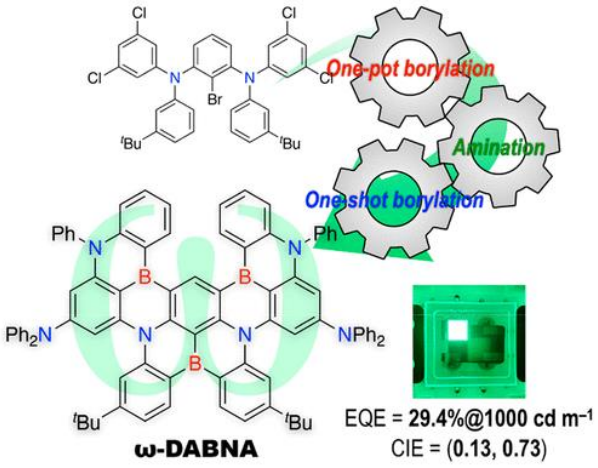

Figure 17. A sequential borylation reaction including one-pot borylation, amination, and one-shot borylation for the construction of highly efficient MR-TADF molecule of **ω-DABNA** containing three boron atoms. Reproduced with permission.[101] Copyright 2023, American Chemical Society.

Table 1. Summary of photophysical properties for the reported MR TADF emitters with fast $k_{RISC} > 10^5$ s^{-1} in the references.

Compound	λ_{em}[a] (nm)	FWHM[b] (nm)	Φ_{PL}[c] (%)	ΔE_{ST}[d] (eV)	τ_{PF}[e] (ns)	τ_{DF}[f] (μs)	k_{ISC}[g] (10^7 s^{-1})	k_{RISC}[h] (10^5 s^{-1})	$\langle S_n\|\hat{H}_{SOC}\|T_n\rangle$[i] ($cm^{-1}$)	ΔE[j] (meV)	Refs.
Cz-PTZ-BN	510/524	37/50	84/91	0.11	6.3	20.7	5.93	0.81	0.24/0.91/0.59	-	[76]
2Cz-PTZ-BN	505/512	38/48	87/96	0.09	5.0	17.6	9.17	1.05	0.29/0.99/0.67	-	[76]
BN4	500/522	43/50	88/96	0.14	5.1	8.3	5.2	1.6	0.01/1.07/-	-	[77]
BN5	497/512	44/49	87/92	0.14	5.1	23.1	8.0	0.74	0.01/1.07/-	-	[77]
2PTZBN	510/519	39/44	58/80	0.15/	4.2	5.0	6.67	2.76	0.02/1.52/1.19	-	[78]
CzBS	471/472	28/30	99/98	0.11/0.14	4.6	30	19	2.2	0.27/0.82/1.47	153	[79]
Cz-BSN	476/-	24/33	-/82	0.13	4.8	40.8	-	0.96	0.25/0.46/-	126	[80]
DCz-BSN	463/-	26/30	-/88	0.12	4.8	49.1	-	1.04	0.30/0.43/-	115	[80]
SBSN	489/-	27/-	-/76	0.10	8.9	32.2	9.5	1.5	0.15/0.63/1.09	-	[81]
DBSN	553/-	28/-	-/98	0.13	4.3	25.7	18.7	1.9	0.01/0.29/-	-	[81]
DBNS	631/-	40/-	80/-	0.20	14.4	11.2	-	2.1	0.07/1.38/-	169	[82]
DBNS-*t*Bu	641/-	39/-	85/-	0.19	19.1	10.2	-	2.2	0.10/1.43/-	163	[82]
BSBS-N1	473/478	21/24	59/89	0.13/0.14	0.9	5.6	100	19	0.31/0.35/1.41	-	[83]
BOBS-Z	453/457	21/24	94/93	0.16/0.12	1.1	7.6	78	8.6	0.38/1.34/1.18		[84]
BSBS-Z	460/464	20/22	93/88	0.14/0.12	1.0	6.7	9.2	16	0.47/1.01/1.75		[84]
BSS	457/-	27/-	-/58	0.15	11.0	85.1	-	1.18	0.77/0.32/-	190	[85]
PS-BSS	456/-	30/-	-/59	-	8.9	67.0	-	-	-/-/-	-	[85]
PAc-BSS	455/-	30/-	-/60	-	9.0	71.9	-	-	-/-/-	-	[85]
CzBSe	477/479	33/34	98/98	0.12/0.15	0.8	14	110	1800	0.87/4.78/10.8	172	[79]
Cz-BSeN	479/-	30/-	-/87	0.15	0.9	29.8	110	75	1.96/2.51/3.48	134	[86]
DCz-BSeN	472/-	28/-	-/93	0.14	0.7	28.4	140	88	2.52/3.96/9.42	123	[86]
BN-Se	502/505	42/44	99/98	0.08	0.9	5.2	100	16	1.50/0.48/5.15	450	[87]
BNSSe	505/520	39/-	-/99	0.12	3.0	12.7	29	6	1.58/2.06/0.91	-	[48]
BNSeSe	502/514	38/-	-/100	0.14	1.9	9.9	49	20	1.43/2.84/2.11	-	[48]
BN-STO	506/517	29/34	93/96	0.13	5.4	25.3	12.5	1.2	1.61/1.07/0.12	-	[88]
Cl-MR	460/474	27/36	-/85	0.14/0.13	4.1	17	9.8	0.98	0.06/0.68	-	[89]
Br-MR	460/474	27/36	-/76	0.14/0.13	1.0	9.9	83	5.9	0.19/2.21	-	[89]
(SIPr)AuBN	511/515	30/37	88/92	0.07	-	5.5	-	230	-/-/-	-	[52, 90]
(IPr)AuBN	511/514	31/37	83/90	0.08	-	5.8	300	33	-/-/-	-	[90]
(BzIPr)AuBN	511/513	30/37	86/91	0.09	-	5.5	310	50	1.67/-/-	-	[90]
(PyIPr)AuBN	511/514	30/37	93/88	0.08	-	5.9	310	32	-/-/-	-	[90]
(PzIPr)AuBN	510/514	30/37	78/87	0.08	-	5.6	-	-	-/-/-	-	[90]
(BzIPr)AuBNO	471/473	30/37	89/84	0.11	-	22.8	320	11	-/-/-	-	[90]
BNCPPt	497/507	27/35	75/49	-	-	-	-	-	2.82/17.97/3.84	150	[91]
v-DABNA	468/467	14/18	74/90	0.02	4.1	4.1	2.3	2.0	0.03/0.05/-	-	[32]
m-v-DABNA	464/-	14/-	-/90.5	0.07	8.43	3.09	2.55	2.30	-/-/-	-	[92]

4F-v-DABNA	457/-	14/-	-/90.2	0.05	8.72	3.12	2.52	2.28	-/-/-	-	[92]
4F-m-v-DABNA	455/-	14/-	-/88.9	0.07	8.20	3.19	2.79	2.10	-/-/-	-	[92]
v-DABNA-CN-Me	496/-	17/-	86/-	0.03	4.9	10	0.8	1.0	0.04/0.16/-	-	[93]
v-DABNA-O-Me	461/464	19/24	90/90	0.12	5.1	7.7	4.0	1.6	0.03/0.05/-	-	[94]
BN3	456/458	17/21	-/98	0.15	1.3	17.8	61.9	2.55	0.10/1.14/0.20	82	[95]
NO-DBMR	458/-	14/-	-/83.4	0.04	2.02	1.44	4.16	1.04	0.02/0.14/0.05	-	[96]
Cz-DBMR	480/-	14/-	-/82.1	0.04	5.06	2.18	4.55	3.72	0.05/0.18/0.07	-	[96]
DBTN-2	512/-	20/-	-/100	0.06	3.5	6.5	2.2	1.7	0.15/0.46/-	-	[97]
DTBA-BN2	490/496	41/46	96/97	0.13	6.3	4.2	-	2.3	-/-/-	-	[98]
DTBA-B2N3	471/476	23/26	97/96	0.10	2.4	1.1	-	16	-/-/-	-	[98]
***m*-DBCz**	541/-	32/-	95/-	0.04	4.2	14..8	13.1	16.5	0.03/0.63/0.04	-	[99]
TPD4PA	445/-	19/-	-/88.1	0.05	7.82	4.69	5.14	2.51	0.10/0.33/-	-	[100]
tBu-TPD4PA	451/-	19/-	-/90.3	0.06	8.07	5.55	5.30	2.44	0.12/0.39/-	-	[100]
VTCzBN	496/-	34/-	-/98	0.06	3.3	9.9	27	10	0.15/0.94/0.52	-	[70]
TCz-VTCzBN	521/-	29/-	-/98	<0.01	13.2	8.7	6	9	0.29/0.27/0.22	-	[70]
V-DABNA-Mes	486/484	13/16	79/80	0.005	7.0	2.4	0.73	4.4	-/-/-	-	[101]
V-DABNA	483/481	14/17	85/90	0.006	6.9	1.9	1.1	5.7	0.01/0.08/-	-	[102]
V-DABNA-F	467/464	13/16	91/81	0.005	6.6	1.7	1.4	6.5	0.01/0.09/-	-	[102]
ω-DABNA	509/509	18/22	92/87	0.013	5.9	8.9	0.1	1.2	-/-/-	-	[103]
CzB4	-/483	-/14	-/91.6	0.0042	5.29	5.02	2.7	1.8	0.25/0.003/-		[104]
CzB6	-/488	-/12	-/94.0	0.0031	3.34	2.93	3.4	3.0	0.339/0.000/-		[104]
CzB8	-/491	-/12	-/92.2	0.003	3.14	1.41	4.8	6.5	0.344/0.034/-		[104]
CzB4-oPh	-/478	-/12	-/92.5	0.0087	5.24	16.0	3.7	0.64	-/-/-		[104]

[a] Maximum emission peak in solution and film. [b] Full width at half-maximum values for emission in solution and film. [c] Photoluminescence quantum yields in solution and film. [d] Singlet-triplet energy gap. [e] Emission lifetime of prompt fluorescence. [f] Emission lifetime of delayed fluorescence. [g] Intersystem crossing rate constant. [h] Reverse intersystem crossing rate constant. [i] Simulated spin-orbit coupling constants of S_1-T_1, S_1-T_2 and S_1-T_3. [j] Simulated total reorganization energy.

Table 2. Summary of device performance for OLEDs using the MR TADF emitters with fast $k_{RISC} > 10^5$ s^{-1} as emitter.

Compound	V_{on}[a] (V)	λ_{EL}[b] (nm)	FWHM[c] (nm)	L[d] (cd m^{-2})	CE[e] (cd A^{-1})	PE[f] (lm W^{-1})	EQE[g] (%)	Roll-off[h] (%)	CIE[i] (x, y)	Refs.
Cz-PTZ-BN	3.3	520	54	29793	100.4/-/-	86.1/-/-	27.6/26.2/17.3	5.1/37.3	(0.26, 0.65)	[76]
2Cz-PTZ-BN	3.3	516	56	26887	108.5/-/-	92.1/-/-	32.8/30.8/23.5	6.1/28.4	(0.24, 0.63)	[76]
(+)-BN4	4.4	510	49	3334	66.30/-/-	38.58/-/-	20.6/20.5/10.7	0.5/48.1	(0.186, 0.632)	[77]
(-)-BN4	4.4	512	49	3037	55.05/-/-	35.16/-/-	19.0/16.6/10.1	12.6/46.8	(0.206, 0.635)	[77]
(+)-BN5	4.8	506	48	2950	65.12/-/-	36.47/-/-	22.0/15.3/10.9	30.4/50.5	(0.173, 0.590)	[78]
(-)-BN5	4.8	506	48	3062	79.37/-/-	44.46/-/-	26.5/17.6/11.1	33.6/58.1	(0.167, 0.603)	[79]
2PTZBN	3.0	528	58	16720	96.5/-/-	86.6/-/-	25.5/21.7/17.2	14.9/32.5	(0.28, 0.65)	[80]

CzBS	4.0	473	31	-	25.8/-/-	19.4/-/-	23.1/21.3/15.0	7.8/35.1	(0.11, 0.16)	[80]
Cz-BSN	3.6	482	32	4034	29.5/21.0/10.6	-/-/-	18.9/13.4/6.8	29.1/64.0	(0.11, 0.28)	[81]
DCz-BSN	3.8	473	29	4397	25.7/20.3/11.7	-/-/-	22.0/18.6/10.0	15.5/54.6	(0.11, 0.17)	[81]
SBSN	3.4	492	31	22817	40.4/40.4/27.5	25.4/25.4/13.9	17.6/17.6/12.0	0.0/31.8	(0.10, 0.44)	[82]
DBSN	3.7	556	43	15484	84.7/80.0/65.8	71.9/55.8/37.6	21.8/20.6/16.9	5.5/22.5	(0.42, 0.57)	[82]
DBNS*	3.7	613	66	4345	7.2/-/5.4	-/-/-	5.8/-/4.4	-/24.1	(0.64, 0.34)	[83]
DBNS-*t*Bu*	3.5	616	65	5694	9.2/-/6.9	-/-/-	7.8/-/5.8	-/25.6	(0.65, 0.34)	[84]
BSBS-N1	-	478	25	-	-/-/-	-/-/-	21.0/-/-	-/-	(0.11, 0.22)	[84]
BOBS-Z	4.0	456	23	-	16.7/-/-	12.9/-/-	26.9/24.0/15.0	10.8/44.2	(0.14, 0.06)	[85]
BSBS-Z	4.0	463	22	-	23.2/-/-	15.0/-/-	26.8/24.0/15.9	10.4/40.7	(0.13, 0.08)	[85]
PAc-BSS*	3.3	458	31	1328	17.7/-/-	13.0/-/-	13.1/-/-	-/-	(0.16, 0.12)	[85]
CzBSe	3.9	481	33	-	34.8/-/-	25.8/-/-	23.9/23.4/20.0	2.1/16.3	(0.10, 0.24)	[79]
Cz-BSeN	3.3	490	36	11251	44.0/36.7/29.7	39.8/25.0/15.4	20.3/16.9/13.7	16.7/32.5	(0.13, 0.45)	[86]
DCz-BSeN	3.5	481	32	6875	32.3/28.4/22.6	28.0/18.7/12.0	22.3/19.6/15.6	12.1/30.0	(0.11, 0.44)	[86]
BN-Se	2.4	506	45	> 10^5	95.9/-/-	103.9/-/-	32.6/-/32.2	-/1.3	(0.15, 0.62)	[87]
BNSSe	2.4	515	50	113881	124.2/-/110.8	156.2/-/90.2	35.7/-/32.0	-/10.4	(0.22, 0.66)	[48]
BNSeSe	2.4	512	48	108188	121.0/-/111.0	146.3/-/90.1	36.8/-/34.0	-/7.6	(0.19, 0.66)	[48]
BN-STO	2.4	517	34	93313	141.2/-/-	176.9/-/-	40.1/39.0/28.1	2.7/29.9	(0.19, 0.70)	[88]
Cl-MR	4.2	472	30	209	-/-/-	-/-/-	17.0/-/-	-/-	(0.12, 0.19)	[89]
Br-MR	5.0	476	39	10.3	-/-/-	-/-/-	4.2/-/-	-/-	(0.14, 0.25)	[89]
(SIPr)AuBN	-	511	40	253000	86.1/-/84.4	-/-/-	24.8/-/24.3	-/2.0	(0.20, 0.69)	[52, 90]
(IPr)AuBN	-	509	35	117000	74.0/-/62.0	-/-/-	24.0/-/20.2	-/15.8	(0.16, 0.66)	[90]
(BzIPr)AuBN	-	510	34	216000	97.1/-/89.9	-/-/-	30.3/-/28.1	-/7.3	(0.16, 0.68)	[90]
(PyIPr)AuBN	-	512	37	151000	93.5/-/69.3	-/-/-	27.6/-/20.5	-/25.7	(0.18, 0.69)	[90]
(PzIPr)AuBN	-	515	39	192000	82.8/-/79.7	-/-/-	24.0/-/23.1	-/3.8	(0.22, 0.67)	[90]
v-DABNA	3.4	469	18	-	31.0/29.5/23.2	25.6/20.8/11.7	34.4/32.8/26.0	1.6/8.6	(0.12, 0.11)	[32]
m-*v*-DABNA	3.7	471	18	-	32.1/18.6[j]	-/-/-	36.2/20.4[k]	43.6[l]	(0.12, 0.12)	[92]
4F-*v*-DABNA	3.7	464	18	-	26.8/14.7[j]	-/-/-	35.8/16.7[k]	53.4[l]	(0.13, 0.08)	[92]
4F-m-v-DABNA	3.7	461	18	-	24.9/13.2[j]	-/-/-	33.7/17.9[k]	46.9[l]	(0.13, 0.06)	[92]
***v*-DABNA-CN-Me**	3.2	504	23	-	89.0/87.1/78.2	137.6/135.3/122.3	32.0/31.5/28.5	0.4/3.4	(0.13, 0.65)	[93]
v-DABNA-O-Me	3.4	465	23	-	24.6/23.8/22.1	22.7/17.7/13.5	29.5/28.8/26.9	0.7/2.6	(0.13, 0.10)	[94]
BN3	4.1	458	23	18438	27.5/-/-	19.0/-/-	37.6/34.0/26.2	9.6/30.3	(0.14, 0.08)	[95]
NO-DBMR	3.6	469	26	-	29.2/-/-	-/-/-	33.7/-/-	-/-	(0.12, 0.12)	[96]
Cz-DBMR	3.6	491	22	-	42.3/-/-	-/-/-	29.8/-/-	-/-	(0.09, 0.34)	[96]
DBTN-2	2.8	520	29	42180	132.9/127.0/78.1	130.4/115.6/56.0	35.2/33.6/20.4	4.6/42.0	(0.19, 0.74)	[97]
DTB-BN2	-	497	47	-	-/-/-	58.8/-/-	31.2/28.2/25.6	9.6/18.0	(0.13, 0.49)	[98]
DTB-B2N3	-	475	28	-	-/-/-	28.1/-/-	30.9/27.4/20.5	11.3/33.7	(0.11, 0.18)	[98]
m-DBCz	3.3	548	35	109087	145.8/-/-	134.2/-	34.9/-/31.3	-/10.3	(0.35, 0.63)	[99]
TPD4PA	3.1	455	29	-	15.7/-/9.2	-/-/-	30.7/30.6/17.8	0.3/42.0	(0.14, 0.06)	[100]
tBu-TPD4PA	3.1	469	29	-	19.4/-/12.9	-/-/-	32.5/30.9/20.5	4.9/36.9	(0.14, 0.07)	[100]
VTCzBN	3.9	499	38	31691	91.0/71.4/56.9	66.4/48.7/33.1	31.7/24.8/19.8	21.8/37.5	(0.14, 0.56)	[70]
TCz-VTCzBN	3.8	524	37	38657	129.3/72.2/64.2	96.7/49.3/37.3	32.2/18.0/16.0	44.1/50.3	(0.22, 0.71)	[70]
V-DABNA-Mes	3.2	480	27	-	26.7[m]/24.2/12.9	20.0[n]/12.6/4.5	22.9[o]/20.3/10.9	11.4/52.4[p]	(0.09, 0.21)	[101]
V-DABNA	3.4	483	17	-	36.2/35.6/34.1	33.1/26.1/20.9	26.2/26.2/25.3	0.1/0.9	(0.09, 0.27)	[102]
V-DABNA-F	3.2	468	15	-	22.3/21.3/19.2	21.5/15.7/11.4	26.6/25.8/23.4	3.0/12.0	(0.12, 0.10)	[102]

ω-DABNA	3.2	512	25	-	101.8/101.0/95.9	88.8/82.5/67.0	31.1/30.8/29.4	1.0/1.7	(0.13, 0.73)	[103]
CzB4-oPh	3.2	490	21	-	57.0/55.0/50.8	55.9/44.0/33.8	28.7/27.8/25.8	3.1/10.1	(0.09, 0.45)	[104]

[a] Turn-on voltage at luminance of 1 cd m^{-2}. [b] Maximum electroluminescence peak. [c] Full width at half-maximum values of electroluminescence. [d] Maximum luminance. [e] Current efficiency (CE): maximum, values at 100 and 1000 cd m^{-2}. [f] Power efficiency (PE): maximum, values at 100 and 1000 cd m^{-2}. [g] External quantum efficiency (EQE): maximum, values at 100 and 1000 cd m^{-2}. [h] EQE roll-offs at 100 and 1000 cd m^{-2} from maximum EQE. [i] Commission International de L'Eclairage coordinate. [j] CE at 400 cd m^{-2}. [k] EQE at 400 cd m^{-2}. [l] EQE roll-off at 400 cd m^{-2} from maximum EQE. [m] CE at 10 cd m^{-2}. [n] PE at 10 cd m^{-2}. [o] EQE at 10 cd m^{-2}. [p] EQE roll-offs at 100 and 1000 cd m^{-2} from EQE at 10 cd m^{-2}. * OLED fabricated by solution-process.

6. Summary and outlook

The increasing awareness of the benefit of optoelectronics has triggered a growing demand in high-performance organic semiconductor. With the unique advantages of both 100% internal quantum efficiency in theory and narrowband emission, MR-TADF emitters have attracted considerable attention. As a result, the molecular design and the device performance of MR-TADF emitters have witnessed a great progress since the pioneer work in 2016. In this review, we summarized the recent advances of MR-TADF materials with fast RISC rate constant (>10^5 s^{-1}) from the perspective of molecular design, photophysical properties and device performance in OLEDs to extract fundamental design principles of high-performance MR-TADF molecules and provide a deep insight into the structure-performance relationship of MR-TADF materials. Although significant advances have been achieved in this field, there are still many challenges in MR-TADF materials and their practical applications in electroluminescent devices that have yet to be addressed.

First, the RISC rate constants of MR-TADF molecules are still slow compared to those for traditional D-A type TADF emitters. The introduction of the heavy atom, such as Se, can significantly accelerate the RISC process, thereby alleviating the efficiency roll-off of OLEDs based on the MR-TADF emitters. However, the widened emission profile will be obtained owing to the large structural relaxation of heavy atom-integrated units with folded configurations; on the other hand, the poor operation lifetime of OLEDs was confirmed, resulting from the weak bond energy between the carbon and heavy atoms.

Second, the type of MR-TADF molecules is rare, which is mainly focused on the B/O, B/N and N/C=O units, severely restricting the expansion of the MR molecular family. The exploration of other possible MR units, such as using the electron-withdrawing phosphine oxide

or sulfone groups, is helpful to understand the structure-performance relationship of the MR-TADF emitters for the flourishing development of the highly efficient OLEDs.

Third, deep-blue MR-TADF molecules are rarely achieved owing to the lack of the specific molecular design strategy and the intrinsic trapping of charge carriers induced by a large band gap. Actually, the MR-TADF molecules containing O-B-N unit usually exhibited blue-shifted emission because of the weak electron-donating ability of oxygen atom, but with a poor device performance. By integrating the asymmetric O-B-N unit into MR-TADF molecules to form a more rigid skeleton, this can significantly improve the performance of deep-blue OLEDs, providing a feasible strategy of molecular design for high-performance deep-blue MR-TADF OLEDs.

Fourth, there is a huge challenge in the development of deep-red and near-infared (DR/NIR) MR-TADF molecules. For organic emitters, extending the π-conjugation length is an effective way to red-shift the emission. However, the non-bonding characters of MR cores limited the increase of conjugation. Enhancing the CT character in MR-TADF emitters is an alternative way to achieve red-shifted emissions, which would inevitably weaken the MR effect and thus broaden the emission spectra. Therefore, designing the DR/NIR MR-TADF emitters is still in its infancy. The strategies in this review can provide some ideas in terms of fastening the reverse intersystem crossing rate and narrowing the emission profile for future DR/NIR MR-TADF emitters.

Fifth, the extension of MR skeleton is beneficial for narrowing the emission profile and lowering the ΔE_{ST}, but the inevitably increased molecular weight makes the process with vacuum evaporation difficult, which requires more precise equipment. The synthesis of the extended MR-TADF molecules is not mature yet as well.

To overcome these problems, we believe that the innovative molecular design is one of the entrances to achieve high-performance MR-TADF emitters, which should possess simultaneously small ΔE_{ST}, high PLQY and large RISC rate constant with high stability and processability. For example, we can achieve that by developing novel MR units or integrating heavy atom into the extended MR units. Moreover, new theoretical models and challenging views for predicting the properties of MR-TADF molecules could have a profound effect on the development of high-performance MR-TADF optoelectronic materials. Besides, the optimization of the device configuration and the improvement of the device fabrication would promote the fast development of OLEDs based on MR-TADF emitters. Based on the systematic reviews and analyses on the progress of MR-TADF molecules, we believe that this review article can guide the pathways for designing high-performance MR-TADF emitters with both

high color purity and fast RISC rate to speed up the development of organic optoelectronic materials.

Acknowledgements

This work was supported by the National Key Technologies R&D Program of China (2022YFE0104100), National Natural Science Foundation of China (22205188), ITC Guangdong-Hong Kong Technology Cooperation Funding Scheme (TCFS) (GHP/038/19GD), CAS-Croucher Funding Scheme for Joint Laboratories (ZH4A), the Hong Kong Research Grants Council (PolyU 15305320), the Hong Kong Polytechnic University (YXB8), Miss Clarea Au for the Endowed Professorship in Energy (847S), and Research Institute for Smart Energy (CDAQ).

Conflicts of Interest

The authors declare no conflict of interest.

References

[1] C. W. Tang, S. A. VanSlyke, *Appl. Phys. Lett.* **1987**, *51*, 913.

[2] M. Pope, H. P. Kallmann, P. Magnante, *J. Chem. Phys.* **1963**, *38*, 2042.

[3] C. Adachi, M. A. Baldo, M. E. Thompson, S. R. Forrest, *J. Appl. Phys.* **2001**, *90*, 5048.

[4] X. Ai, E. W. Evans, S. Dong, A. J. Gillett, H. Guo, Y. Chen, T. J. H. Hele, R. H. Friend, F. Li, *Nature* **2018**, *563*, 536.

[5] H. Xu, R. Chen, Q. Sun, W. Lai, Q. Su, W. Huang, X. Liu, *Chem. Soc. Rev.* **2014**, *43*, 3259.

[6] J. Bian, S. Chen, L. Qiu, R. Tian, Y. Man, Y. Wang, S. Chen, J. Zhang, C. Duan, C. Han, H. Xu, *Adv. Mater.* **2022**, *34*, e2110547.

[7] H. J. Cheon, S. J. Woo, S. H. Baek, J. H. Lee, Y. H. Kim, *Adv. Mater.* **2022**, *34*, 2207416.

[8] P. Jiang, J. Miao, X. Cao, H. Xia, K. Pan, T. Hua, X. Lv, Z. Huang, Y. Zou, C. Yang, *Adv. Mater.* **2022**, *34*, e2106954.

[9] N. Aizawa, Y. J. Pu, Y. Harabuchi, A. Nihonyanagi, R. Ibuka, H. Inuzuka, B. Dhara, Y. Koyama, K. I. Nakayama, S. Maeda, F. Araoka, D. Miyajima, *Nature* **2022**, *609*, 502.

[10] C.-Y. Chan, M. Tanaka, Y.-T. Lee, Y.-W. Wong, H. Nakanotani, T. Hatakeyama, C. Adachi, *Nat. Photonics* **2021**, *15*, 203.

[11] Z. Yang, Z. Mao, Z. Xie, Y. Zhang, S. Liu, J. Zhao, J. Xu, Z. Chi, M. P. Aldred, *Chem. Soc. Rev.* **2017**, *46*, 915.

[12] H. Y. Park, A. Maheshwaran, C. K. Moon, H. Lee, S. S. Reddy, V. G. Sree, J. Yoon, J. W. Kim, J. H. Kwon, J. J. Kim, S. H. Jin, *Adv. Mater.* **2020**, *32*, e2002120.

[13] P. Sun, D. Liu, F. Zhu, D. Yan, *Nat. Photonics* **2023**, *17*, 264.

[14] M. A. Baldo, D. F. O'Brien, Y. You, A. Shoustikov, S. Sibley, M. E. Thompson, S. R. Forrest, *Nature* **1998**, *395*, 151.

[15] J. Lee, H. F. Chen, T. Batagoda, C. Coburn, P. I. Djurovich, M. E. Thompson, S. R. Forrest, *Nat. Mater.* **2016**, *15*, 92.

[16] J. Sun, H. Ahn, S. Kang, S.-B. Ko, D. Song, H. A. Um, S. Kim, Y. Lee, P. Jeon, S.-H. Hwang, Y. You, C. Chu, S. Kim, *Nat. Photonics* **2022**, *16*, 212.

[17] A. Endo, M. Ogasawara, A. Takahashi, D. Yokoyama, Y. Kato, C. Adachi, *Adv. Mater.* **2009**, *21*, 4802.

[18] Y. Tao, K. Yuan, T. Chen, P. Xu, H. Li, R. Chen, C. Zheng, L. Zhang, W. Huang, *Adv. Mater.* **2014**, *26*, 7931.

[19] Y. Liu, C. Li, Z. Ren, S. Yan, M. R. Bryce, *Nat. Rev. Mater.* **2018**, *3*, 18020.

[20] J. Li, T. Nakagawa, J. MacDonald, Q. Zhang, H. Nomura, H. Miyazaki, C. Adachi, *Adv. Mater.* **2013**, *25*, 3319.

[21] H. Uoyama, K. Goushi, K. Shizu, H. Nomura, C. Adachi, *Nature* **2012**, *492*, 234.

[22] Q. Zhang, D. Tsang, H. Kuwabara, Y. Hatae, B. Li, T. Takahashi, S. Y. Lee, T. Yasuda, C. Adachi, *Adv. Mater.* **2015**, *27*, 2096.

[23] D. Di, A. S. Romanov, L. Yang, J. M. Richter, J. P. Rivett, S. Jones, T. H. Thomas, M. Abdi Jalebi, R. H. Friend, M. Linnolahti, M. Bochmann, D. Credgington, *Science* **2017**, *356*, 159.

[24] X. Tang, L.-S. Cui, H.-C. Li, A. J. Gillett, F. Auras, Y.-K. Qu, C. Zhong, S. T. E. Jones, Z.-Q. Jiang, R. H. Friend, L.-S. Liao, *Nat. Mater.* **2020**, *19*, 1332.

[25] M. Y. Wong, E. Zysman-Colman, *Adv. Mater.* **2017**, *29*, 1605444.

[26] K. Wang, C. J. Zheng, W. Liu, K. Liang, Y. Z. Shi, S. L. Tao, C. S. Lee, X. M. Ou, X. H. Zhang, *Adv. Mater.* **2017**, *29*, 1701476.

[27] T.-L. Wu, M.-J. Huang, C.-C. Lin, P.-Y. Huang, T.-Y. Chou, R.-W. Chen-Cheng, H.-W. Lin, R.-S. Liu, C.-H. Cheng, *Nat. Photonics* **2018**, *12*, 235.

[28] X. Cai, S.-J. Su, *Adv. Funct. Mater.* **2018**, *28*, 1802558.

[29] J. H. Kim, J. H. Yun, J. Y. Lee, *Adv. Optical Mater.* **2018**, *6*, 1800255.

[30] J. Xue, Q. Liang, R. Wang, J. Hou, W. Li, Q. Peng, Z. Shuai, J. Qiao, *Adv. Mater.* **2019**, *31*, e1808242.

[31] T. Hatakeyama, K. Shiren, K. Nakajima, S. Nomura, S. Nakatsuka, K. Kinoshita, J. Ni, Y. Ono, T. Ikuta, *Adv. Mater.* **2016**, *28*, 2777.

[32] Y. Kondo, K. Yoshiura, S. Kitera, H. Nishi, S. Oda, H. Gotoh, Y. Sasada, M. Yanai, T.

Hatakeyama, *Nat. Photonics* **2019**, *13*, 678.

[33] H. Hirai, K. Nakajima, S. Nakatsuka, K. Shiren, J. Ni, S. Nomura, T. Ikuta, T. Hatakeyama, *Angew. Chem. Int. Ed.* **2015**, *54*, 13581.

[34] M. Hirai, N. Tanaka, M. Sakai, S. Yamaguchi, *Chem. Rev.* **2019**, *119*, 8291.

[35] H. J. Kim, T. Yasuda, *Adv. Optical Mater.* **2022**, *10*, 2201714.

[36] T. Fan, Y. Zhang, D. Zhang, L. Duan, *Chem. Eur. J.* **2022**, *28*, e202104624.

[37] K. R. Naveen, H. I. Yang, J. H. Kwon, *Commun. Chem.* **2022**, *5*, 149.

[38] Q. Wang, Y. Xu, T. Yang, J. Xue, Y. Wang, *Adv. Mater.* **2022**, *35*, 2205166.

[39] Y. Xu, Q. Wang, X. Cai, C. Li, Y. Wang, *Adv. Mater.* **2021**, *33*, e2100652.

[40] M. Yang, I. S. Park, T. Yasuda, *J. Am. Chem. Soc.* **2020**, *142*, 19468.

[41] J. Liu, Y. Zhu, T. Tsuboi, C. Deng, W. Lou, D. Wang, T. Liu, Q. Zhang, *Nat. Commun*. **2022**, *13*, 4876.

[42] Z. P. Yan, L. Yuan, Y. Zhang, M. X. Mao, X. J. Liao, H. X. Ni, Z. H. Wang, Z. An, Y. X. Zheng, J. L. Zuo, *Adv. Mater.* **2022**, *34*, e2204253.

[43] X. Cai, J. Xue, C. Li, B. Liang, A. Ying, Y. Tan, S. Gong, Y. Wang, *Angew. Chem. Int. Ed.* **2022**, *134*, e202200337.

[44] J. Park, J. Lim, J. H. Lee, B. Jang, J. H. Han, S. S. Yoon, J. Y. Lee, *ACS Appl. Mater. Interfaces* **2021**, *13*, 45798.

[45] S. Madayanad Suresh, D. Hall, D. Beljonne, Y. Olivier, E. Zysman-Colman, *Adv. Funct. Mater.* **2020**, *30*, 1908677.

[46] J. Han, Z. Huang, X. Lv, J. Miao, Y. Qiu, X. Cao, C. Yang, *Adv. Optical Mater.* **2021**, *10*, 2102092.

[47] J. M. dos Santos, D. Sun, J. M. Moreno-Naranjo, D. Hall, F. Zinna, S. T. J. Ryan, W. Shi, T. Matulaitis, D. B. Cordes, A. M. Z. Slawin, D. Beljonne, S. L. Warriner, Y. Olivier, M. J. Fuchter, E. Zysman-Colman, *J. Mater. Chem. C* **2022**, *10*, 4861.

[48] Y. X. Hu, J. Miao, T. Hua, Z. Huang, Y. Qi, Y. Zou, Y. Qiu, H. Xia, H. Liu, X. Cao, C. Yang, *Nat. Photonics* **2022**, *16*, 803.

[49] M. Mońka, I. E. Serdiuk, K. Kozakiewicz, E. Hoffman, J. Szumilas, A. Kubicki, S. Y. Park, P. Bojarski, *J. Mater. Chem. C* **2022**, *10*, 7925.

[50] H. S. Kim, J. Y. Lee, S. Shin, W. Jeong, S. H. Lee, S. Kim, J. Lee, M. C. Suh, S. Yoo, *Adv. Funct. Mater.* **2021**, *31*, 2170374.

[51] S. Gan, S. Hu, X. L. Li, J. Zeng, D. Zhang, T. Huang, W. Luo, Z. Zhao, L. Duan, S. J. Su, B. Z. Tang, *ACS Appl. Mater. Interfaces* **2018**, *10*, 17327.

[52] J. Wang, N. Li, C. Zhong, J. Miao, Z. Huang, M. Yu, Y. X. Hu, S. Luo, Y. Zou, K. Li, C.

Yang, *Adv. Mater.* **2022**, *35*, 202208378.

[53] S. Oda, W. Kumano, T. Hama, R. Kawasumi, K. Yoshiura, T. Hatakeyama, *Angew. Chem. Int. Ed.* **2021**, *60*, 2882.

[54] S. M. Suresh, E. Duda, D. Hall, Z. Yao, S. Bagnich, A. M. Z. Slawin, H. Bassler, D. Beljonne, M. Buck, Y. Olivier, A. Kohler and E. Zysman-Colman, *J. Am. Chem. Soc.* **2020**, *142*, 6588.

[55] K. Matsui, S. Oda, K. Yoshiura, K. Nakajima, N. Yasuda, T. Hatakeyama, *J. Am. Chem. Soc.* **2018**, *140*, 1195.

[56] S. Chen, H. Xu, *Chem. Soc. Rev.* **2021**, *50*, 8639.

[57] A. K. Pal, S. Krotkus, M. Fontani, C. F. R. Mackenzie, D. B. Cordes, A. M. Z. Slawin, I. D. W. Samuel, E. Zysman-Colman, *Adv. Mater.* **2018**, *30*, e1804231.

[58] D. Karthik, Y. H. Jung, H. Lee, S. Hwang, B. M. Seo, J. Y. Kim, C. W. Han, J. H. Kwon, *Adv. Mater.* **2021**, *33*, e2007724.

[59] T. A. Lin, T. Chatterjee, W. L. Tsai, W. K. Lee, M. J. Wu, M. Jiao, K. C. Pan, C. L. Yi, C. L. Chung, K. T. Wong, C. C. Wu, *Adv. Mater.* **2016**, *28*, 6976.

[60] G. Xie, J. Wang, X. Xue, H. Li, N. Guo, H. Li, D. Wang, M. Li, W. Huang, R. Chen, Y. Tao, *Appl. Phys. Rev.* **2022**, *9*, 031410.

[61] L.-S. Cui, A. J. Gillett, S.-F. Zhang, H. Ye, Y. Liu, X.-K. Chen, Z.-S. Lin, E. W. Evans, W. K. Myers, T. K. Ronson, H. Nakanotani, S. Reineke, J.-L. Bredas, C. Adachi, R. H. Friend, *Nat. Photonics* **2020**, *14*, 636.

[62] Y. Wada, H. Nakagawa, S. Matsumoto, Y. Wakisaka, H. Kaji, *Nat. Photonics* **2020**, *14*, 643.

[63] D. H. Ahn, S. W. Kim, H. Lee, I. J. Ko, D. Karthik, J. Y. Lee, J. H. Kwon, *Nat. Photonics* **2019**, *13*, 540.

[64] T. Chen, L. Zheng, J. Yuan, Z. An, R. Chen, Y. Tao, H. Li, X. Xie, W. Huang, *Sci. Rep.* **2015**, *5*, 10923.

[65] T. J. Penfold, E. Gindensperger, C. Daniel, C. M. Marian, *Chem. Rev.* **2018**, *118*, 6975.

[66] X. Luo, L. Zhang, Y. Zheng, L. Ding, *J. Semicond.* **2022**, *43*, 110202.

[67] X. Zeng, L. Wang, H. Dai, T. Huang, M. Du, D. Wang, D. Zhang, L. Duan, *Adv. Mater.* **2023**, 2211316.

[68] X. Liang, Z. P. Yan, H. B. Han, Z. G. Wu, Y. X. Zheng, H. Meng, J. L. Zuo, W. Huang, *Angew. Chem. Int. Ed.* **2018**, *57*, 11316.

[69] X. Cai, Y. Xu, Y. Pan, L. Li, Y. Pu, X. Zhuang, C. Li, Y. Wang, *Angew. Chem. Int. Ed.* **2022**, *62*, e202216473.

[70] X. F. Luo, S. Q. Song, H. X. Ni, H. Ma, D. Yang, D. Ma, Y. X. Zheng, J. L. Zuo, *Angew.*

Chem. Int. Ed. **2022**, *61*, e202209984.

[71] A. Pershin, D. Hall, V. Lemaur, J. C. Sancho-Garcia, L. Muccioli, E. Zysman-Colman, D. Beljonne, Y. Olivier, *Nat. Commun*. **2019**, *10*, 597.

[72] C. M. Marian, *WIREs Comput. Mol. Sci*. **2012**, *2*, 187.

[73] W. Zhao, Z. He, Jacky W. Y. Lam, Q. Peng, H. Ma, Z. Shuai, G. Bai, J. Hao, Ben Z. Tang, *Chem* **2016**, *1*, 592.

[74] K. N. Solov'ev, E. A. Borisevich, *Phys.-Usp.* **2005**, *48*, 231.

[75] M. Einzinger, T. Zhu, P. de Silva, C. Belger, T. M. Swager, T. Van Voorhis, M. A. Baldo, *Adv. Mater.* **2017**, *29*, 1701987.

[76] P. Lu, F. Liu, Z. Cheng, Y. Jiang, L. Gao, H. Liu, H. Liu, Z. Feng, W. Yang, *Angew. Chem. Int. Ed.* **2022**, *61*, e202116927.

[77] X. Wu, J. W. Huang, B. K. Su, S. Wang, L. Yuan, W. Q. Zheng, H. Zhang, Y. X. Zheng, W. Zhu, P. T. Chou, *Adv. Mater.* **2022**, *34*, e2105080.

[78] T. Hua, L. Zhan, N. Li, Z. Huang, X. Cao, Z. Xiao, S. Gong, C. Zhou, C. Zhong, C. Yang, *Chem. Eng. J.* **2021**, *426*, 131169.

[79] I. S. Park, H. Min, T. Yasuda, *Angew. Chem. Int. Ed.* **2022**, *134*, e202205684.

[80] Q. Li, Y. Wu, X. Wang, Q. Yang, J. Hu, R. Zhong, S. Shao, L. Wang, *Chem. Eur. J.* **2022**, *28*, e202104214.

[81] X. F. Luo, H. X. Ni, A. Q. Lv, X. K. Yao, H. L. Ma, Y. X. Zheng, *Adv. Optical Mater.* **2022**, *10*, 2200504.

[82] Y. Wang, K. Zhang, F. Chen, X. Wang, Q. Yang, S. Wang, S. Shao, L. Wang, *Chin. J. Chem.* **2022**, *40*, 2671.

[83] M. Nagata, H. Min, E. Watanabe, H. Fukumoto, Y. Mizuhata, N. Tokitoh, T. Agou, T. Yasuda, *Angew. Chem. Int. Ed.* **2021**, *60*, 20280.

[84] I. S. Park, M. Yang, H. Shibata, N. Amanokura, T. Yasuda, *Adv. Mater.* **2021**, *34*, e2107951.

[85] F. Chen, L. Zhao, X. Wang, Q. Yang, W. Li, H. Tian, S. Shao, L. Wang, X. Jing, F. Wang, *Sci. China Chem.* **2021**, *64*, 547.

[86] Q. Li, Y. Wu, Q. Yang, S. Wang, S. Shao, L. Wang, *ACS Appl. Mater. Interfaces* **2022**, *14*, 49995.

[87] X. Cao, K. Pan, J. Miao, X. Lv, Z. Huang, F. Ni, X. Yin, Y. Wei, C. Yang, *J. Am. Chem. Soc.* **2022**, *144*, 22976.

[88] Y. Hu, J. Miao, C. Zhong, Y. Zeng, S. Gong, X. Cao, X. Zhou, Y. Gu, C. Yang, *Angew. Chem. Int. Ed.* **2023**, *62*, e202302478.

[89] Y. Lee, J.-I. Hong, *J. Mater. Chem. C* **2022**, *10*, 11855.

[90] S. Cai, G. S. M. Tong, L. Du, G. K. So, F. F. Hung, T. L. Lam, G. Cheng, H. Xiao, X. Chang, Z. X. Xu, C. M. Che, *Angew. Chem. Int. Ed.* **2022**, *61*, e202213392.

[91] Y. Feng, X. Zhuang, Y. Xu, J. Xue, Q. Wang, Y. Liu, Y. Wang, *ChemRxiv* **2023**, https://doi.org/10.26434/chemrxiv-2023-qfsdc.

[92] K. Rayappa Naveen, H. Lee, R. Braveenth, K. Joon Yang, S. Jae Hwang, J. Hyuk Kwon, *Chem. Eng. J.* **2022**, *432*, 134381.

[93] S. Oda, T. Sugitani, H. Tanaka, K. Tabata, R. Kawasumi, T. Hatakeyama, *Adv. Mater.* **2022**, *34*, 2201778.

[94] H. Tanaka, S. Oda, G. Ricci, H. Gotoh, K. Tabata, R. Kawasumi, D. Beljonne, Y. Olivier, T. Hatakeyama, *Angew. Chem. Int. Ed.* **2021**, *60*, 17910.

[95] X. Lv, J. Miao, M. Liu, Q. Peng, C. Zhong, Y. Hu, X. Cao, H. Wu, Y. Yang, C. Zhou, J. Ma, Y. Zou, C. Yang, *Angew. Chem. Int. Ed.* **2022**, *134*, e202201588.

[96] K. R. Naveen, J. H. Oh, H. Lee, J. H. Kwon, *Angew. Chem. Int. Ed.* **2023**, doi: 10.1002/anie.202306768.

[97] X.-C. Fan, K. Wang, Y.-Z. Shi, Y.-C. Cheng, Y.-T. Lee, J. Yu, X.-K. Chen, C. Adachi, X.-H. Zhang, *Nat. Photonics* **2023**, *17*, 280.

[98] B. Lei, Z. Huang, S. Li, J. Liu, Z. Bin, J. You, *Angew. Chem. Int. Ed.* **2023**, *135*, e202218405.

[99] X. Cai, Y. Pu, C. Li, Z. Wang, Y. Wang, *Angew. Chem. Int. Ed.* **2023**, *62*, e202304104.

[100] K. R. Naveen, H. Lee, L. H. Seung, Y. H. Jung, C. P. Keshavananda Prabhu, S. Muruganantham, J. H. Kwon, *Chem. Eng. J.* **2023**, *451*, 138498.

[101] S. Oda, B. Kawakami, Y. Yamasaki, R. Matsumoto, M. Yoshioka, D. Fukushima, S. Nakatsuka, T. Hatakeyama, *J. Am. Chem. Soc.* **2022**, *144*, 106.

[102] S. Oda, B. Kawakami, M. Horiuchi, Y. Yamasaki, R. Kawasumi, T. Hatakeyama, *Adv. Sci.* **2022**, *10*, e2205070.

[103] S. Uemura, S. Oda, M. Hayakawa, R. Kawasumi, N. Ikeda, Y. T. Lee, C. Y. Chan, Y. Tsuchiya, C. Adachi, T. Hatakeyama, *J. Am. Chem. Soc.* **2023**, 145, 1505.

[104] Y. Sano, T. Shintani, M. Hayakawa, S. Oda, M. Kondo, T. Matsushita, T. Hatakeyama, *J. Am. Chem. Soc.* **2023**, *145*, 11504.

He Jiang received her Ph.D. degree from The Nanjing University of Posts and Telecommunications in 2021. She is currently a postdoctoral fellow in Prof. Wai-Yeung Wong's group. Her research interests include the novel molecular design, synthesis and optoelectronic characterization of molecules toward highly efficient organic electroluminescence devices.

Jibiao Jin received his Ph.D. degree from The Nanjing University of Posts and Telecommunications in 2020. He is currently a postdoctoral fellow in Prof. Wai-Yeung Wong's group. His current research focuses on the development of high-performance multi-resonance thermally activated delayed fluorescence (MR-TADF) materials.

Wai-Yeung Wong received his Ph.D. degree from The University of Hong Kong in 1995. He is currently Chair Professor of Chemical Technology, Clarea Au Professor in Energy, and Dean of the Faculty of Science at The Hong Kong Polytechnic University. He is the President of the Hong Kong Chemical Society. He is also the recipient of the RSC Chemistry of the Transition Metals Award from the United Kingdom, State Natural Science Award (second-class) from

China, and RGC Senior Research Fellow Award from Hong Kong, among others. His research interest focuses on the design, synthesis, and application of metallopolymers, metallophosphors, and metal-based nanomaterials.